

High-order spline finite element method for solving time-dependent electromagnetic waves

Imad El-Barkani^a, Imane El-Hadouti^a, Mohamed Addam^{a,c,*}, Mohammed Seaid^b

^aUniversité Abdelmalek Essaadi, EMAO, LSA, ENSAH, BP 03, 32003 Ajdir, Al Hoceima, Morocco

^bDepartment of Engineering, University of Durham, South Road, DH1 3LE, United Kingdom

^cUniversité du Littoral Côte d'Opale, L.M.P.A, 50 rue F. Buisson BP699, F-62228 Calais-Cedex, France

Abstract

In this paper we propose a high-order spline finite element method for solving a class of time-dependent electromagnetic waves and its associated frequency-domain approach. A Fourier transform and its inverse are used for the time integration of the wave problem. The spatial discretization is performed using a partitioned mesh with tensorial spline functions to form bases of the discrete solution in the variational finite element space. Quadrature methods such as the Gauss-Hermite quadrature are implemented in the inverse Fourier transform to compute numerical solutions of the time-dependent electromagnetic waves. In the present study we carry out a rigorous convergence analysis and establish error estimates for the wave solution in the relevant norms. We also provide a full algorithmic description of the method and assess its performance by solving several test examples of time-dependent electromagnetic waves with known analytical solutions. The method is shown to verify the theoretical estimates and to provide highly accurate and efficient simulations. We also evaluate the computational performance of the proposed method for solving a problem of wave transmission through non-homogeneous materials. The obtained computational results confirm the excellent convergence, high accuracy and applicability of the proposed spline finite element method.

Keywords: Electromagnetic waves; Frequency-domain approach; B -splines; Finite element method; Quadrature methods; Error and convergence analysis.

1. Introduction

Electromagnetic wave problems have been investigated by several researchers in engineering and scientific computing communities for many years regarding their fundamental importance in various applications including mobile communications, medical imaging devices and electrical power generation among others, see for example [1, 2, 3]. Other applications related to wave propagations include mechanical waves in solids and fluids, seismic waves, geophysics waves, acoustic waves and the Maxwell problems describing the propagation of electromagnetic waves, see [4, 5, 6] among others. In these later problems, the electromagnetic signal is recovered by solving the linear Maxwell equations for which the induced electric and magnetic fields are also solutions of these equations, see for instance [7, 8, 9, 10]. Time-harmonic wave problems governed by the Helmholtz equation have also been largely studied in the literature, see [3, 11, 12, 13, 14, 6, 5, 2, 15, 10] among others. Solving time-dependent wave problems using the conventional finite element methods is challenging due to the hyperbolic nature of the governing equations and the presence of high wavenumbers making the standard Galerkin techniques inaccurate and inefficient. Therefore, numerous computational techniques have been designed to deal with this class of problems such as finite difference methods [16, 17], finite element methods [18, 19, 20, 21, 22, 23], finite volume methods [24, 25] and boundary element methods

*Corresponding author

Email addresses: imad.elbarkani@etu.uae.ac.ma (Imad El-Barkani), imane.elhadouti@etu.uae.ac.ma (Imane El-Hadouti), m.addam@uae.ac.ma (Mohamed Addam), m.seaid@durham.ac.uk (Mohammed Seaid)

[7, 8]. It is also well known that these methods do not perform very satisfactory in the case of wave problems with high wavelengths unless highly refined meshes are adopted in the spatial discretization or high-order basis functions are used in the solution approximation. Nevertheless, these methods are also known to suffer from dispersion errors when applied to wave problems, see for example [26]. In this reference, a failure to resolve the precise wavelength does not only reflect on the fine details of the numerical solution, but it also contaminates its global features in the time domain. This property widely known by the pollution error in computational acoustics [27] and it cannot be fully eliminated in wave problems but, it can be reduced by either refining the mesh or increasing the polynomial degree used in the approximation [28]. However, as the problem involves time dependency, employing high-order time integration schemes is vital in these methods to achieve consistent convergence rates in both spatial and temporal discretizations, see [29] and further discussions are therein. Needless to mention that using explicit time stepping in these methods on fine meshes would require extremely small time steps to maintain stability of the computed solutions. Combining high-order methods for the spatial discretization with low-order time integration schemes might turn out inefficient for numerically addressing transient wave problems. To overcome these drawbacks without compromising the accuracy, a frequency-domain approach using the Fourier transform and its inverse for the time integration is adopted in the current study.

Spline functions are well recognized as effective tools in approximation theory, computer design, diagnostic imaging among other engineering applications, see for instance [30, 31, 32, 33, 32, 34, 35, 36, 37, 38, 39]. The conceptual theory of polynomial spline functions is also well established in the literature and widely used in vast areas of engineering, see [40, 33, 31, 32, 41, 34, 35] among others. The spline functions are also well known in the field of computer aided geometric design and computer graphics however, their applications in finite element analysis have not been widely implemented for solving partial differential equations governing electromagnetic waves. For example, detailed formulation of the Bernstein-Bézier representation of basis polynomials can be found in [30], and polynomial splines have also been used as basis functions for the finite element methods, see for example [42, 43]. The polynomial spline functions have also been used by researchers in geoscience as new tools for approximation and data fitting on the sphere [31]. Implementing Non-Uniform Rational B-Splines (NURBS) to replace the standard polynomials in finite element methods has also been widely used in the framework of isogeometric analysis, see for example [44]. This enables the description of the geometry using the NURBS and their use in computing the numerical solution, even with relatively coarse elements that can accurately depict complex geometries. On the other hand, Normalized Uniform Polynomial Spline (NUPS) functions are of high importance in approximation theory, and ideal for computer-aided geometric design or finite element methods, see for example [41]. It should be stressed that these hierarchical basis functions are often chosen in the design of high-order finite elements for their suitability in p -adaptivity. Recently, attention has been paid to the favorable properties of tensioned splines instead of NURBS or B-splines.

In the present study we are interested in solving time-dependent electromagnetic waves using a novel high-order spline finite element method. This class of problems occurs in many engineering applications for which the hyperbolic equation has been used as a standard model for describing the propagation of waves. Therefore, accurate and reliable numerical approximations of these hyperbolic wave equations are of a fundamental importance to the simulations. In the current work, the two-dimensional wave problems are solved to recover the non-stationary electromagnetic signal also known by the magnitude density of the transverse-electric field or by simply the transverse-magnetic field. The proposed method employs the frequency-domain approach based on the Fourier transform which leads to an intermediate differential equation depending on the frequency variable. This class of techniques avoid finite difference approximations in time by using the Fourier transform and its inverse for the time integration, see [45, 46] for similar techniques. Notice that when solving time-dependent problems using finite element methods, significant consideration should be given to the choice of time integration schemes, especially when using high-order spatial discretization. The selection of time integration for time-dependent electromagnetic waves strongly depends on values of the wave number and the mesh refinement. If the wave number and mesh refinements are very high, spurious oscillations due to numerical dispersion can occur in the solution with explicit solvers, whereas the computational cost in the implicit solvers can be overwhelming. Needless to mention that for this class of time-dependent problems, employing high-order time integration schemes becomes

imperative to achieve consistent convergence rates in both spatial and temporal dimensions [29]. In the present study, to eliminate these drawbacks associated with time integration for wave problems, we consider the frequency-domain approach using Fourier transform and its inverse. It should also be stressed that the Fourier transform and its inverse are considered as isometric isomorphisms between the Hilbert spaces such as those considered here for solving wave problems. This isomorphism is also known as Fourier-Plancherel and it allows a robust approximation using quadrature methods to calculate the solution of the inverse Fourier transform. Therefore, this results in a stable, simple and efficient algorithm for solving time-dependent electromagnetic waves using high-order spline finite element discretizations for the space. Note that, although the considered frequency-domain formulation requires the use of the Fourier transform and the associated inverse, its implementation is generally simpler than for the time-domain formulation. Our main objective in the current work consists in developing a class of high-order finite element methods to numerically solve time-dependent electromagnetic wave problems. This is achieved by solving the resulting frequency-domain problem by a finite element method employing the high-order \mathbb{B}_γ -splines as basis functions with the arbitrary order γ . By their regularities in $\mathcal{C}^{\gamma-1}$, the proposed \mathbb{B}_γ -spline functions are ideal in the field of approximation and computer-aided geometric design. In the framework of finite element methods, the high-order \mathbb{B}_γ -spline functions would provide smooth macro-element spaces which are required for accurate solutions of time-dependent electromagnetic waves particularly at high wavelengths. In addition, using the \mathbb{B}_γ -spline functions, we can generate the mass and stiffness matrices globally on all the nodes of the mesh instead of working on a reference element which requires transformation mappings. Therefore, unlike other high-order spline functions, when used within the finite element approximations, the proposed high-order \mathbb{B}_γ -splines yield sparse matrices with the added tridiagonal structure. Once, the magnitude density is obtained in the frequency-domain problem, quadrature methods including the Gauss-Hermite quadrature are used to compute the time-domain magnitude density as an inverse Fourier transform with respect to the time variable. To the best of our knowledge, solving the time-dependent electromagnetic wave problems using these techniques is reported for the first time. It should be stressed that the model considered in this work represents the principal reference basis of many linear electromagnetic and acoustic problems. For instance, applied to separate components of the linear electromagnetic field, it can represent an accurate and efficient solution for a short pulse propagating over long distances. We also develop a rigorous analysis of convergence for this method and provide error estimates for the wave solution in the relevant norms. To examine the accuracy of the proposed high-order spline finite element method, we present numerical results for several wave problems with known exact solutions and also for a problem of wave transmission through non-homogeneous materials. The obtained results for different wavenumbers are in good agreement with the theoretical error estimates and illustrate good numerical features in terms of stability and high accuracy.

The paper is organized as follows: In section 2, governing equations for time-dependent electromagnetic waves are presented. This section also includes the notations along with functional spaces and assumptions used in the present study. The proposed high-order spline finite element method is formulated in section 3. In this section, we present the frequency-domain variational formulation, introduce the high-order tensor-product splines, and reconstruct the solution of the inverse Fourier transform. Section 4 presents the convergence analysis for the proposed spline finite element method and establishes the error estimates for the wave solution in the relevant norms. Numerical results obtained for several examples of time-dependent electromagnetic waves are illustrated in section 5. Finally, we conclude with some remarks and recommendations for future work in section 6.

2. Governing equations for time-dependent electromagnetic waves

Let $\Omega \subset \mathbb{R}^2$ be an open bounded domain with Lipschitz continuous boundary $\partial\Omega$ and let $[0, T]$ be the time interval for the wave propagation with T is the final time. We also denote by $\mathbf{x} = (x, y)^\top \in \Omega$ the cartesian coordinates and by $\phi(\mathbf{x}, t)$ the magnitude density of the transverse electromagnetic field at the position $\mathbf{x} \in \Omega$ and at the time $t \in [0, T]$. In the present study, we are interested in the dynamics of transverse electromagnetic waves for the magnitude density of the transverse electric field or the reconstruction of transverse magnetic fields. Thus, the hyperbolic deterministic transverse electromagnetic wave equation

satisfied by the magnitude density $\phi(\mathbf{x}, t)$ in the direction perpendicular to the domain plane is given by

$$\frac{1}{v^2(\mathbf{x})} \frac{\partial^2 \phi}{\partial t^2}(\mathbf{x}, t) - \nabla^2 \phi(\mathbf{x}, t) = f(\mathbf{x}, t), \quad (\mathbf{x}, t) \in \Omega \times [0, T], \quad (1)$$

equipped with the initial conditions

$$\phi(\mathbf{x}, 0) = \phi_0(\mathbf{x}), \quad \text{and} \quad \frac{\partial \phi}{\partial t}(\mathbf{x}, 0) = \phi_1(\mathbf{x}), \quad \mathbf{x} \in \Omega, \quad (2)$$

where ϕ_0 and ϕ_1 are given initial functions. In (1), $v(\mathbf{x}) = \frac{v_0}{\nu(\mathbf{x})}$ is the speed function of sound with v_0 is the speed of sound in the vacuum, ν is the reflective index of the domain, and $f(\mathbf{x}, t)$ presents the internal source term. On the boundary $\partial\Omega$, we assume absorbing boundary conditions as

$$\frac{\rho(\hat{\mathbf{x}})}{v(\hat{\mathbf{x}})} \frac{\partial \phi}{\partial t}(\hat{\mathbf{x}}, t) + \beta(\hat{\mathbf{x}})\phi(\hat{\mathbf{x}}, t) + \frac{\partial \phi}{\partial \mathbf{n}}(\hat{\mathbf{x}}, t) = g(\hat{\mathbf{x}}, t), \quad (\hat{\mathbf{x}}, t) \in \partial\Omega \times [0, T], \quad (3)$$

where β is a bounded function on the boundary $\partial\Omega$, ρ is a non-negative bounded weight function on $\partial\Omega$, $\mathbf{n}(\hat{\mathbf{x}})$ is the outward unit normal at $\hat{\mathbf{x}}$ on $\partial\Omega$ and $g(\hat{\mathbf{x}}, t)$ is a given boundary function, see for example [47] for more details on these parameters. Throughout this study, we assume that the real-valued function β is a positive bounded function belonging to the canonical space $L^\infty(\partial\Omega)$. In addition, v , ρ and β are assumed to be positive bounded functions belonging to the space $L^\infty(\bar{\Omega})$ *i.e.*, there exist positive constants v_{max} , v_{min} , ρ_{max} and β_{max} such that

$$0 < v_{min} \leq v(x) \leq v_{max}, \quad 0 \leq \rho(x) \leq \rho_{max}, \quad \text{and} \quad 0 \leq \beta(x) \leq \beta_{max}, \quad \forall \mathbf{x} \in \bar{\Omega}, \quad (4)$$

with $\bar{\Omega} = \Omega \cup \partial\Omega$. In the sequel, we use the following notations: the classical space of square integrable complex-valued functions on the domain Ω is denoted by $\widehat{L}_2 := L^2(\Omega, \mathbb{C})$ and it is endowed by its natural topology defined by the following inner product and its associated norm

$$(u|v)_2 = \int_{\Omega} u(x)\overline{v(x)}dx, \quad \|u\|_2 = \sqrt{(u|u)_2}, \quad \forall u, v \in \widehat{L}_2.$$

For every $k \in \mathbb{N}$, we also denote by $\widehat{H}_k := W^{k,2}(\Omega, \mathbb{C})$ the usual Sobolev space equipped with the classical norm $\|\cdot\|_{\widehat{H}_k}$ given by

$$\|u\|_{\widehat{H}_k} = \left(\sum_{|\ell| \leq k} \|\partial^\ell u\|_2^2 \right)^{\frac{1}{2}}, \quad \forall u \in \widehat{H}_k, \quad (5)$$

where $\partial^\ell u := \partial^{\ell_1} \dots \partial^{\ell_d} u$ stands for the derivative (in the distribution sense) of the function u of order $|\ell| = \sum_{i=1}^d \ell_i$ and $\partial^{\ell_i} = \frac{\partial^{\ell_i}}{\partial x_i^{\ell_i}}$, for $i = 1, \dots, d$. The classical space of square integrable real-valued functions on the domain Ω is denoted by $L_2 := L^2(\Omega, \mathbb{R})$ and H_k denotes the canonical Sobolev space of real-valued functions defined by $H_k := W^{k,2}(\Omega, \mathbb{R})$ and equipped with the classical norm $\|\cdot\|_{H_k}$ given in (5). The classical space $L^2(\Omega, \mathbb{R})$ of square integrable real-valued functions in the domain Ω is denoted by $L_2 := L^2(\Omega, \mathbb{R})$ and H_m denotes the Sobolev space of real-valued functions defined by $H_m = H^m(\Omega, \mathbb{R}) := W^{m,2}(\Omega, \mathbb{R})$ and equipped with the classical norm $\|\cdot\|_{H_m}$ defined in (5). Let m be an integer, we consider the Schwartz space $\mathcal{S}(\mathbb{R}; H_m)$ and the space $\mathcal{S}'(\mathbb{R}; H_m)$ of the tempered distributions, namely the linear and continuous forms from $\mathcal{S}(\mathbb{R}; H_m)$ into \mathbb{R} is the topological dual of the space $\mathcal{S}(\mathbb{R}; H_m)$. Similarly, for every $s \in \mathbb{R}$, we consider the space $H^s(\mathbb{R}; \mathbb{R})$ and the non-homogeneous Sobolev spaces $H^s(\mathbb{R}; H_m)$, for more detail on these spaces we refer to [45, 46].

We assume that the magnitude density $t \mapsto \phi(\mathbf{x}, t)$ and its gradient $t \mapsto \nabla \phi(\mathbf{x}, t)$ have extensions in \mathbb{R} which belong respectively, to the spaces $L^1(\mathbb{R}, \mathbb{R})$ and $(L^1(\mathbb{R}, \mathbb{R}))^2$ almost everywhere in Ω . We also assume

that the source terms f and g have extensions, still denoted by f and g , such that $f \in L^\infty(\Omega; L^1(\mathbb{R}, \mathbb{R}))$ and $g \in L^\infty(\partial\Omega; L^1(\mathbb{R}, \mathbb{R}))$. Recall that the Fourier transform $\widehat{\psi}$ of a function ψ in $L^1(\mathbb{R}, \mathbb{R})$ is given by

$$\widehat{\psi}(\omega) = \frac{1}{\sqrt{2\pi}} \int_{-\infty}^{+\infty} \psi(t) e^{-i\omega t} dt, \quad i = \sqrt{-1}. \quad (6)$$

By using the Lebesgue theorem of derivation under the integral sign [48], we obtain

$$\widehat{\nabla\phi}(x, \omega) = \nabla\widehat{\phi}(x, \omega), \quad \forall (x, \omega) \in \Omega \times \mathbb{R}. \quad (7)$$

Hence, we apply the Fourier transform to the equation (1) along with the non-homogeneous Robin-type boundary conditions (3), we use the classical relation $\widehat{\frac{\partial\psi}{\partial t}} = i\omega\widehat{\psi}$ and the relation (7) to obtain an elliptic wave equation satisfied by the transverse electromagnetic wave in the frequency-domain as

$$-\left(\nabla^2 + \frac{\omega^2}{v^2(\mathbf{x})}\right) u(\mathbf{x}, \omega) = F(\mathbf{x}, \omega), \quad (\mathbf{x}, \omega) \in \Omega \times \mathbb{R}, \quad (8)$$

subject to the following absorbing boundary condition

$$\frac{i\omega}{v(\widehat{\mathbf{x}})} \rho(\widehat{\mathbf{x}}) u(\widehat{\mathbf{x}}, \omega) + \beta(\widehat{\mathbf{x}}) u(\widehat{\mathbf{x}}, \omega) + \frac{\partial u}{\partial \mathbf{n}}(\widehat{\mathbf{x}}, \omega) = G(\widehat{\mathbf{x}}, \omega), \quad (\widehat{\mathbf{x}}, \omega) \in \partial\Omega \times \mathbb{R}, \quad (9)$$

where $u(\cdot, \omega) = \widehat{\phi}(\cdot, \omega)$, $F(\cdot, \omega) = \widehat{f}(\cdot, \omega)$ and $G(\cdot, \omega) = \widehat{g}(\cdot, \omega)$ are the Fourier transforms with respect to the time variable t of $\phi(\mathbf{x}, \cdot)$, $f(\mathbf{x}, \cdot)$ and $g(\widehat{\mathbf{x}}, \cdot)$, respectively.

3. High-order spline finite element method

In this section we formulate the proposed high-order spline finite element method for solving the wave problem (8)-(9). We first present the variational formulation of the problem and then we introduce the high-order tensor-product splines. We also present the inverse Fourier transform to reconstruct the time-dependent solution of the transverse electromagnetic wave problem.

3.1. Frequency-domain variational formulation

Let $u_*(\cdot, \omega)$ be a sufficiently smooth function (for instance $u_*(\cdot, \omega) \in \widehat{\mathbf{H}}_1$) solving the problem (8)-(9). Hence, multiplying the wave equation (8) by an arbitrary function $\bar{v} \in \widehat{\mathbf{H}}_1$, integrating over Ω and using the Green-Gauss theorem with the non-homogeneous Robin-type boundary conditions (9), the weak variational formulation associated with the transverse electromagnetic wave problem in the frequency-domain reads

$$\mathcal{A}_\omega(u(\cdot, \omega), v) = \mathcal{L}_\omega(v), \quad \forall v \in \widehat{\mathbf{H}}_1, \quad (10)$$

where the sesquilinear form $\mathcal{A}_\omega : \widehat{\mathbf{H}}_1 \times \widehat{\mathbf{H}}_1 \rightarrow \mathbb{C}$ and the semi-linear form $\mathcal{L}_\omega : \widehat{\mathbf{H}}_1 \rightarrow \mathbb{C}$ are defined for all $u, v \in \widehat{\mathbf{H}}_1$ by

$$\mathcal{A}_\omega(u, v) = -\omega^2 \int_{\Omega} \frac{1}{v^2(\mathbf{x})} u(\mathbf{x}) \overline{v(\mathbf{x})} d\mathbf{x} + \int_{\Omega} \nabla u(\mathbf{x}) \overline{\nabla v(\mathbf{x})} d\mathbf{x} + \oint_{\partial\Omega} \left(\beta(\widehat{\mathbf{x}}) + \frac{i\omega}{v(\widehat{\mathbf{x}})} \rho(\widehat{\mathbf{x}}) \right) u(\mathbf{x}) \overline{v(\widehat{\mathbf{x}})} d\widehat{\mathbf{x}}, \quad (11)$$

and

$$\mathcal{L}_\omega(v) = \int_{\Omega} F(\mathbf{x}, \omega) \overline{v(\mathbf{x})} d\mathbf{x} + \oint_{\partial\Omega} G(\widehat{\mathbf{x}}, \omega) \overline{v(\widehat{\mathbf{x}})} d\widehat{\mathbf{x}}, \quad (12)$$

respectively. Conversely, let $u_*(\cdot, \omega) \in \widehat{\mathbf{H}}_1$ satisfying the weak variational formulation (10), then it follows from the Green-Gauss theorem that

$$\int_{\Omega} \left(-\left(\nabla^2 + \frac{\omega^2}{v^2(\mathbf{x})}\right) u(\mathbf{x}, \omega) - F(\mathbf{x}, \omega) \right) \overline{v(\mathbf{x})} d\mathbf{x} = \oint_{\partial\Omega} \left(\frac{i\omega}{v(\widehat{\mathbf{x}})} \rho(\widehat{\mathbf{x}}) u(\widehat{\mathbf{x}}, \omega) + \beta(\widehat{\mathbf{x}}) u(\widehat{\mathbf{x}}, \omega) + \frac{\partial u}{\partial \mathbf{n}}(\widehat{\mathbf{x}}, \omega) - G(\widehat{\mathbf{x}}, \omega) \right) \overline{v(\widehat{\mathbf{x}})} d\widehat{\mathbf{x}},$$

for all $v \in \widehat{H}_1$. Particularly, for every C^∞ -function φ with compact support in Ω , it yields

$$\int_{\Omega} \left(- \left(\nabla^2 + \frac{\omega^2}{v^2(\mathbf{x})} \right) u(\mathbf{x}, \omega) - F(\mathbf{x}, \omega) \right) \overline{\varphi(\mathbf{x})} d\mathbf{x} = 0.$$

Thus, in the distribution sense, we have

$$- \left(\nabla^2 + \frac{\omega^2}{v^2(\mathbf{x})} \right) u(\mathbf{x}, \omega) = F(\mathbf{x}, \omega), \quad \forall \mathbf{x} \in \overline{\Omega}.$$

Since the function f is assumed to be in $L^\infty(\Omega; L^1(\mathbb{R}, \mathbb{R}))$, it follows that $F(\cdot, \omega)$ belongs to the space $L^\infty(\Omega, \mathbb{C})$. Hence, the previous equality holds almost everywhere in Ω and therefore, for every C^∞ -function φ compactly supported in $\partial\Omega$, we have

$$\oint_{\partial\Omega} \left(\frac{i\omega}{v(\hat{\mathbf{x}})} \rho(\hat{\mathbf{x}}) u(\hat{\mathbf{x}}, \omega) + \beta(\hat{\mathbf{x}}) u(\hat{\mathbf{x}}, \omega) + \frac{\partial u}{\partial \mathbf{n}}(\hat{\mathbf{x}}, \omega) - G(\hat{\mathbf{x}}, \omega) \right) \overline{\varphi(\hat{\mathbf{x}})} d\hat{\mathbf{x}} = 0.$$

Next, let $K \subset \partial\Omega$ be a compact set and \mathcal{K} be a neighborhood of K such that $K \subset \mathcal{K} \subset \partial\Omega$. According to the Urysohn Lemma [49, 50], there exists a compactly supported C^∞ -function φ_c in $\partial\Omega$ satisfying $\varphi_c(\hat{\mathbf{x}}) = 1$ on \mathcal{K} and $\varphi_c(\hat{\mathbf{x}}) = 0$ outside of \mathcal{K} . Hence, taking $\varphi = \varphi_c$ in the above equation, we obtain for every compact subset K in $\partial\Omega$

$$\oint_{\mathcal{K}} \left(\frac{i\omega}{v(\hat{\mathbf{x}})} \rho(\hat{\mathbf{x}}) u(\hat{\mathbf{x}}, \omega) + \beta(\hat{\mathbf{x}}) u(\hat{\mathbf{x}}, \omega) + \frac{\partial u}{\partial \mathbf{n}}(\hat{\mathbf{x}}, \omega) - G(\hat{\mathbf{x}}, \omega) \right) d\hat{\mathbf{x}} = 0.$$

It follows that

$$i\omega \frac{\rho(\cdot)}{v(\cdot)} u(\cdot, \omega) + \beta(\cdot) u(\cdot, \omega) + \frac{\partial u}{\partial \mathbf{n}}(\cdot, \omega) = G(\cdot, \omega), \quad a.e. \text{ on } \partial\Omega.$$

It is evident that, the problem (8)-(9) is equivalent to the weak variational formulation (10) and, from the trace theorem, there exists a constant $M_1 > 0$ (depending only on Ω) such that

$$\|u\|_{L^2(\partial\Omega, \mathbb{C})} \leq M_1 \|u\|_{\widehat{H}_1}, \quad \forall u \in \widehat{H}_1. \quad (13)$$

Using the Schwarz inequality and the Sobolev continuous embedding theorem, it follows that there exists a constant $M_2 > 0$ (depending only on $\partial\Omega$) such that

$$|\mathcal{L}_\omega(v)| \leq \mathcal{R}(\omega) \|v\|_{\widehat{H}_1}, \quad \forall v \in \widehat{H}_1, \quad (14)$$

where $\mathcal{R}(\omega) = M_2 \left(\|F(\cdot, \omega)\|_{\widehat{L}_2} + \|G(\cdot, \omega)\|_{L^2(\partial\Omega, \mathbb{C})} \right)$. Therefore, the operator $\mathcal{L}_\omega : \widehat{H}_1 \rightarrow \mathbb{C}$ is a continuous semi-linear form in \widehat{H}_1 . Again, using the Sobolev continuous embedding theorem, it yields that there exists a non-negative constant $M_3 > 0$ not depending on the frequency ω such that

$$|\mathcal{A}_\omega(u, v)| \leq M_3(1 + \omega^2) \|u\|_{\widehat{H}_1} \|v\|_{\widehat{H}_1}, \quad \forall u, v \in \widehat{H}_1. \quad (15)$$

Hence, the coercivity of the sesquilinear form \mathcal{A}_ω given in (11) is also ensured by the following Lemma:

Lemma 1. *Let ω be a fixed real frequency, the sesquilinear form \mathcal{A}_ω given in (11) is coercive on a subspace $\mathcal{H} \subseteq \widehat{H}_1$. Furthermore, there exists a constant $\alpha \in]0, 1[$ such that*

$$|\mathcal{A}_\omega(u, u)| \geq \alpha \|u\|_{\widehat{H}_1}^2, \quad (16)$$

for all $u \in \mathcal{H} \subseteq \widehat{H}_1$. \square

PROOF. For every $u \in \widehat{\mathbf{H}}_1$, we have

$$\operatorname{Re}(\mathcal{A}_\omega(u, u)) = -\omega^2 \int_{\Omega} \frac{1}{v^2(\mathbf{x})} |u(\mathbf{x})|^2 d\mathbf{x} + \int_{\Omega} |\nabla u(\mathbf{x})|^2 d\mathbf{x} + \oint_{\partial\Omega} \beta(\hat{\mathbf{x}}) |u(\hat{\mathbf{x}})|^2 d\hat{\mathbf{x}}.$$

Hence,

$$\begin{aligned} |\mathcal{A}_\omega(u, v)| \geq \operatorname{Re}(\mathcal{A}_\omega(u, u)) &\geq -\omega^2 \int_{\Omega} \frac{1}{v^2(\mathbf{x})} |u(\mathbf{x})|^2 d\mathbf{x} + \int_{\Omega} |\nabla u(\mathbf{x})|^2 d\mathbf{x}, \\ &\geq -\frac{\omega^2}{v_{max}^2} \int_{\Omega} |u(\mathbf{x})|^2 d\mathbf{x} + \int_{\Omega} |\nabla u(\mathbf{x})|^2 d\mathbf{x}. \end{aligned}$$

It is clear that the coercivity bound is satisfied if there is a constant $\alpha > 0$ such that

$$-\frac{\omega^2}{v_{max}^2} \int_{\Omega} |u(\mathbf{x})|^2 d\mathbf{x} + \int_{\Omega} |\nabla u(\mathbf{x})|^2 d\mathbf{x} \geq \alpha \|u\|_{\widehat{\mathbf{H}}_1}^2, \quad (17)$$

which is true here since the following inequality

$$(1 - \alpha) \|\nabla u\|_{\mathbf{L}_2}^2 = (1 - \alpha) \int_{\Omega} |\nabla u(\mathbf{x})|^2 d\mathbf{x} \geq \left(\alpha + \frac{\omega^2}{v_{max}^2} \right) \int_{\Omega} |u(\mathbf{x})|^2 d\mathbf{x} = \left(\alpha + \frac{\omega^2}{v_{max}^2} \right) \|u\|_{\mathbf{L}_2}^2 \geq 0,$$

is satisfied. Hence, there exists a constant $\alpha \in]0, 1[$ such that

$$(1 - \alpha) \|\nabla u(\cdot, \omega)\|_{\mathbf{L}_2}^2 \geq \left(\alpha + \frac{\omega^2}{v_{max}^2} \right) \|u(\cdot, \omega)\|_{\mathbf{L}_2}^2 \geq 0. \quad (18)$$

Let \mathcal{H} be a subspace of functions $u \in \widehat{\mathbf{H}}_1$ satisfying the inequality (18), then it is obvious to obtain the following coercivity bound

$$|\mathcal{A}_\omega(u, u)| \geq \operatorname{Re}(\mathcal{A}_\omega(u, u)) \geq \alpha \|u\|_{\widehat{\mathbf{H}}_1}^2. \quad (19)$$

for all $u \in \mathcal{H}$. \blacksquare

Let ω be a real fixed frequency, and denote by \mathcal{H} the subspace of functions $u(\cdot, \omega) \in \widehat{\mathbf{H}}_1$ that satisfy the inequality (18). Hence, from (15) and (16), the sesquilinear form $\mathcal{A}_\omega : \mathcal{H} \times \mathcal{H} \rightarrow \mathbb{C}$ is continuous and coercive, and from (14) the semi-linear form $\mathcal{L}_\omega : \mathcal{H} \rightarrow \mathbb{C}$ is also continuous. Next, we state the following result:

Theorem 1. *For a fixed frequency ω in \mathbb{R} , the problem (8)-(9) has a unique solution $u_*(\cdot, \omega)$ in \mathcal{H} satisfying*

$$\|u_*(\cdot, \omega)\|_{\widehat{\mathbf{H}}_1} \leq \frac{\mathcal{R}(\mathbf{w})}{\alpha}, \quad (20)$$

where the positive constants α and $\mathcal{R}(\omega)$ are given in (18) and (14), respectively. Furthermore, for $m \geq 2$, if $F(\cdot, \omega)$ is in $C^{m-2}(\overline{\Omega})$, then $u_*(\cdot, \omega) \in C^m(\overline{\Omega})$ is the unique solution of the problem (8)-(9) in the usual sense. \square

PROOF. To establish the results of this theorem, we use the complex version of Lax-Milgram theorem [46] to prove that the problem (8)-(9) has a unique bounded solution. Note that since β is a positive bounded function, the continuity of the semi-linear form $\mathcal{L}_\omega : \widehat{\mathbf{H}}_1 \rightarrow \mathbb{C}$, the continuity and the coercivity of the sesquilinear form $\mathcal{A}_\omega : \widehat{\mathbf{H}}_1 \times \widehat{\mathbf{H}}_1 \rightarrow \mathbb{C}$, by using the complex version of Lax-Milgram theorem [51, 52], imply that there exists a unique solution $u_*(\cdot, \omega)$ of the variational problem (10) in $\widehat{\mathbf{H}}_1$. Since the problem (8)-(9) is equivalent to the variational formulation problem (10), then $u_*(\cdot, \omega)$ is also the unique weak solution of the problem (8)-(9). From the continuity of the operator \mathcal{L}_ω and the coercivity of the operator \mathcal{A}_ω , we have

$$\alpha \|u_*(\cdot, \omega)\|_{\widehat{\mathbf{H}}_1}^2 \leq |\mathcal{A}_\omega(u_*(\cdot, \omega), u_*(\cdot, \omega))| \leq \mathcal{R}(\omega) \|u_*(\cdot, \omega)\|_{\widehat{\mathbf{H}}_1},$$

which yields the inequality (20). Since $u_*(\cdot, \omega) \in \widehat{\mathbf{H}}_1$, then $\nabla u_*(\cdot, \omega) \in (\widehat{\mathbf{L}}_2)^d$. We have $v \in L^\infty(\Omega)$ and $F(\cdot, \omega) \in \widehat{\mathbf{L}}_2$, hence

$$\nabla^2 u_*(\cdot, \omega) = -F(\cdot, \omega) - \frac{\omega^2}{v^2(\cdot)} u_*(\cdot, \omega) \in \widehat{\mathbf{L}}_2. \quad (21)$$

It follows that $\nabla u_*(\cdot, \omega)$ belongs to $(\widehat{\mathbf{H}}_1)^d$ and therefore, the function $u_*(\cdot, \omega)$ belongs to $\widehat{\mathbf{H}}_2$. For $m \geq 2$, if $F(\cdot, \omega) \in C^{m-2}(\overline{\Omega})$ and $v \in C^{m-2}(\overline{\Omega})$, we obtain

$$\nabla^2 u_*(\mathbf{x}, \omega) = -F(\mathbf{x}, \omega) - \frac{\omega^2}{v^2(\mathbf{x})} u_*(\mathbf{x}, \omega), \quad \forall \mathbf{x} \in \overline{\Omega}, \quad (22)$$

in the distribution sense. Using the Sobolev injection, the function $u_*(\cdot, \omega)$ is in $C^{m-2}(\overline{\Omega})$ and by using the assumption that v and $F(\cdot, \omega)$ are in $C^{m-2}(\overline{\Omega})$. Thus, from (22) the weak solution $u_*(\cdot, \omega)$ of the problem (8)-(9) belongs to $C^m(\overline{\Omega})$ and as a consequence, the unique solution of the problem (8)-(9) in the usual sense, see also [53, 52] among others. \blacksquare

3.2. High-order tensor-product splines

For simplicity in the presentation, we consider two-dimensional problems ($d = 2$) such that $\Omega = [a, b] \times [c, d]$ is a rectangular domain. We discretize the interval $[a, b]$ using equally-spaced knot points $x_i = a + ih_1$ for $i = 0, 1, 2, \dots, n_1$ with $h_1 = (b-a)/n_1$, and the interval $[c, d]$ using equally-spaced knot points $y_j = c + jh_2$ for $j = 0, 1, 2, \dots, n_2$ with $h_2 = (d-c)/n_2$. Note that in general, we can consider one mother spline of degree γ and reconstruct a non-uniform discretization of the spatial domain by defining a non-uniform basis for the spatial approximation of the numerical solution. In the present study, for simplicity in the presentation of the proposed algorithm, we consider a uniform partition but the method can also be applied using non-uniform meshes without major conceptual modifications. Let γ be the degree of the considered normalized splines functions, and let us consider the following gridpoints

$$(x_i, y_j) = (a + ih_1, c + jh_2), \quad -\gamma \leq i \leq n_1 - 1, \quad -\gamma \leq j \leq n_2 - 1. \quad (23)$$

We also assume that the domain Ω is covered by an uniform mesh defined by

$$\Omega_h = \{ \mathbf{x}_{ij} = (x_i, y_j)^\top, \ x_i = a + ih_1, \ y_j = c + jh_2, \ i = 0, 1, \dots, n_1, \ j = 0, 1, \dots, n_2 \}, \quad (24)$$

where $h = \max(h_1, h_2)$ is the spatial size of the mesh element $\mathcal{C}_{ij} = [x_i, x_{i+1}] \times [y_j, y_{j+1}]$ in $\overline{\Omega}$ for $0 \leq i \leq n_1 - 1$ and $0 \leq j \leq n_2 - 1$. For a fixed frequency ω in \mathbb{R} , let us denote by $\widehat{\mathcal{V}}_h^{(\gamma, m)}$ the finite dimensional subspace of $\widehat{\mathbf{H}}_m$, given by

$$\widehat{\mathcal{V}}_h^{(\gamma, m)} = \left\{ u_h(\cdot, \omega) \in \widehat{\mathbf{H}}_m : \left. u_h(\cdot, \omega) \right|_{\mathcal{C}_{ij}} \in \mathbb{P}_\gamma \otimes \mathbb{P}_\gamma(\Omega), \quad \text{for } 0 \leq i \leq n_1 - 1, \quad 0 \leq j \leq n_2 - 1 \right\},$$

where $\mathbb{P}_\gamma \otimes \mathbb{P}_\gamma(\Omega)$ is the space of polynomials on Ω of degree $\leq 2\gamma$ and $\gamma \in \mathbb{N}$. It is evident that the dimension of the subspace $\widehat{\mathcal{V}}_h^{(\gamma, m)}$ is $N_\gamma = N_{\gamma,1} N_{\gamma,2}$ where $N_{\gamma,1} = n_1 + \gamma + 2$ and $N_{\gamma,2} = n_2 + \gamma + 2$. To generate a set of basis functions (B_{ij}) for the subspace $\widehat{\mathcal{V}}_h^{(\gamma, m)}$, we use the normalized uniform spline functions \mathbb{B}_γ of degree γ . It should be noted that normalized uniform spline functions are used here only for an algorithmic implementation of the method but spline functions with no normalization property can still be applied. In practice, normalized spline functions would generate matrices with compact and easy structures. Here, the family $(B_{ij} = B_i \otimes B_j)_{\substack{1 \leq i \leq N_{\gamma,1} \\ 1 \leq j \leq N_{\gamma,2}}}$ is the tensorial spline basis functions associated with the given mesh Ω_h . For $i = 1, \dots, N_{\gamma,1}$ and $j = 1, \dots, N_{\gamma,2}$, we have

$$B_{ij}(\mathbf{x}) = B_i \otimes B_j(x, y), \quad \text{for } \mathbf{x} = (x, y)^\top \in \overline{\Omega},$$

and the functions B_i and B_j are defined as

$$B_i(x) = \mathbb{B}_\gamma \left(\frac{x - x_{i-\gamma-1}}{h_1} \right), \quad \text{and} \quad B_j(y) = \mathbb{B}_\gamma \left(\frac{y - y_{j-\gamma-1}}{h_2} \right), \quad (25)$$

where \mathbb{B}_γ is the normalized uniform polynomial spline with the support embedding in the interval $[0, \gamma + 1]$, we refer [46, 33, 31, 32, 41, 34, 35] for more details. It should be stressed that there is no relation between normalized uniform polynomial splines and the spatial discretization of the computational using a uniform mesh. For simplicity in the present work, we construct the splines using a uniform manner based on an algorithm which uses uniform elementary functions. These parent spline functions have bounded supports $[0, \gamma + 1]$ where γ is the degree of the considered spline function. However, non-uniform meshes can still be used in the proposed method for the spatial discretization. Hence, we define a \mathbb{B}_γ -spline basis function for $\gamma = 0$ using the following elementary basis functions $N_{i,\gamma}$ as

$$N_{i,0}(\xi) = \begin{cases} 1, & \text{if } i \leq \xi < i + 1, \\ 0, & \text{otherwise.} \end{cases}$$

For $\gamma \geq 1$, the \mathbb{B}_γ -splines are defined recursively by

$$N_{i,\gamma}(\xi) = \frac{\gamma - i + \xi}{\gamma} N_{i-1,\gamma-1}(\xi) + \frac{i + 1 - \xi}{\gamma} N_{i,\gamma-1}(\xi), \quad (26)$$

for $i = 0, \dots, \gamma - 1$, $\gamma \geq 1$ and $\xi \in [0, 1]$. Note that the fraction of the form $\frac{0}{0}$ in (26) is considered to be zero. It is evident that the elementary functions $N_{k,\gamma}$ are the reference basis of \mathbb{B}_γ -splines and $N_{k,\gamma}$ are normalized such that

$$\sum_{k \in \mathbb{Z}} N_{k,\gamma}(\xi) = 1, \quad \text{for all } \xi \in [0, 1].$$

Thus, the normalized uniform polynomial spline \mathbb{B}_γ of degree $\gamma \in \mathbb{N}$ with the support embedding in $[0, \gamma + 1]$ is defined by

$$\mathbb{B}_\gamma(\zeta) = \begin{cases} N_{\gamma-i,\gamma}(\zeta - k), & \text{for } k \leq \zeta \leq k + 1, \quad k = 0, 1, \dots, \gamma, \\ 0, & \text{for } \zeta \leq 0, \quad \gamma + 1 \leq \zeta. \end{cases}$$

It should also be stressed that the normalized uniform polynomial spline \mathbb{B}_γ of degree γ is a piecewise polynomial with integer knot points and it belongs to $\mathcal{C}^{\gamma-1}$ class of functions. For an illustration, we display in Figure 1 the first \mathbb{B}_γ -spline basis functions for different orders $\gamma = 1, 2, \dots, 10$.

Hence, using the \mathbb{B}_γ -spline basis functions, the subspace $\widehat{\mathcal{V}}_h^{(\gamma,m)}$ is spanned by the tensorial splines functions $(B_{ij} = B_i \otimes B_j)_{\substack{1 \leq i \leq N_{\gamma,1} \\ 1 \leq j \leq N_{\gamma,2}}}$. For $m = 1$, the classical Galerkin approximation consists on finding an approximation $u_h(\cdot, \omega)$ of $u_*(\cdot, \omega)$ as a solution in $\widehat{\mathcal{V}}_h^{(\gamma,1)}$ of the following discrete variational problem

$$\mathcal{A}_\omega(u_h(\cdot, \omega), v_h) = \mathcal{L}_\omega(v_h), \quad \forall v_h \in \widehat{\mathcal{V}}_h^{(\gamma,1)}, \quad (27)$$

where \mathcal{A}_ω and \mathcal{L}_ω are given in (11) and (12), respectively. Note that the solution $u_h(\cdot, \omega)$ of the variational problem (27) can be written in the following form

$$u_h(\mathbf{x}, \omega) = \sum_{i=1}^{N_{\gamma,1}} \sum_{j=1}^{N_{\gamma,2}} Z_{h,ij}(\omega) B_{ij}(\mathbf{x}), \quad \forall \mathbf{x} \in \overline{\Omega}, \quad (28)$$

where $Z_{h,ij}(\omega)$ are complex coefficients with $1 \leq i \leq N_{\gamma,1}$ and $1 \leq j \leq N_{\gamma,2}$. By using the test function $v_h(x, y) = B_{k\ell}(x, y)$ on the weak variational formulation (27), we obtain the Galerkin approximation

$$\sum_{i=1}^{N_{\gamma,1}} \sum_{j=1}^{N_{\gamma,2}} Z_{h,ij}(\omega) A_{ijk\ell}(\omega) = \mathcal{L}_\omega(B_{k\ell}), \quad (29)$$

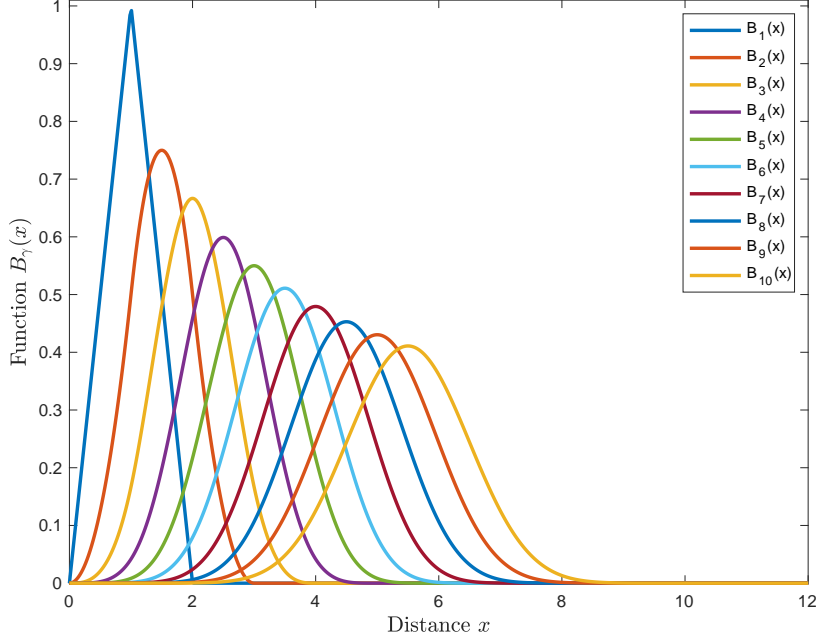


Figure 1: Illustration of \mathbb{B}_γ -spline basis functions with different orders.

for $1 \leq k \leq N_{\gamma,1}$ and $1 \leq \ell \leq N_{\gamma,2}$, where

$$A_{ijkl}(\omega) = \int_c^d \int_a^b (\nabla B_{ij})(x, y) (\nabla B_{kl})(x, y) dx dy + \oint_{\partial\Omega} \beta(\hat{x}, \hat{y}) B_{ij}(\hat{x}, \hat{y}) B_{kl}(\hat{x}, \hat{y}) d\hat{x} d\hat{y} + i\omega \oint_{\partial\Omega} \frac{\rho(\hat{x}, \hat{y})}{v(\hat{x}, \hat{y})} B_{ij}(\hat{x}, \hat{y}) B_{kl}(\hat{x}, \hat{y}) d\hat{x} d\hat{y} - \omega^2 \int_c^d \int_a^b \frac{1}{v^2(x, y)} B_{ij}(x, y) B_{kl}(x, y) dx dy,$$

and

$$\mathcal{L}_\omega(B_{kl}) = \oint_{\partial\Omega} G(\hat{x}, \hat{y}; \omega) B_{kl}(\hat{x}, \hat{y}) d\hat{x} d\hat{y} + \int_\Omega F(x, y; \omega) B_{kl}(x, y) dx dy,$$

for $i, k = 1, 2, \dots, N_{\gamma,1}$ and $j, \ell = 1, 2, \dots, N_{\gamma,2}$. We define $\mathbf{A}(\omega)$ the $N_{\gamma,1}N_{\gamma,2} \times N_{\gamma,1}N_{\gamma,2}$ -valued matrix whose entries are the complex coefficients $A_{ijkl}(\omega) = \mathcal{A}_\omega(B_{ij}, B_{kl})$, $\mathbf{B}_h(\omega)$ the $N_{\gamma,1} \times N_{\gamma,2}$ -valued matrix whose coefficients are $B_{h,kl}(\omega) = \mathcal{L}_\omega(B_{kl})$ and $\mathbf{Z}_h(\omega)$ the $N_{\gamma,1} \times N_{\gamma,2}$ -valued matrix of the unknown complex coefficients $Z_{h,ij}(\omega)$. We also define $\mathbf{b}_h(\omega)$ and $\mathbf{z}_h(\omega)$ as vectors in $\mathbb{C}^{N_{\gamma,1}N_{\gamma,2}}$ the entries of which are the complex coefficients $B_h(\omega)$ and $Z_h(\omega)$, respectively. Hence, the equations (29) can be reformulated in the following $N_{\gamma,1}N_{\gamma,2} \times N_{\gamma,1}N_{\gamma,2}$ linear system

$$\mathbf{A}(\omega)\mathbf{z}_h(\omega) = \mathbf{b}_h(\omega), \quad (30)$$

where for all frequency values ω , the coefficients $Z_{h,ij}(\omega)$ appearing in the the approximate solution u_h of (28) are obtained by solving the linear system (30). The coefficients of the matrix $\mathbf{A}(\omega)$ are evaluated as

$$A_{ijkl}(\omega) = D_{ijkl} + Q_{ijkl} + i\omega \tilde{Q}_{ijkl} - \omega^2 U_{ijkl}, \quad i, k = 1, \dots, N_{\gamma,1} \quad j, \ell = 1, \dots, N_{\gamma,2},$$

where the coefficients D_{ijkl} , U_{ijkl} , Q_{ijkl} and \tilde{Q}_{ijkl} are given by

$$\begin{aligned} D_{ijkl} &= \frac{1}{h_1^2} \int_c^d \int_a^b B'_i(x) B_j(y) B'_k(x) B_\ell(y) dx dy + \frac{1}{h_2^2} \int_c^d \int_a^b B_i(x) B'_j(y) B_k(x) B'_\ell(y) dx dy, \\ U_{ijkl} &= \int_c^d \int_a^b \frac{1}{v^2(x, y)} B_i(x) B_j(y) B_k(x) B_\ell(y) dx dy, \\ Q_{ijkl} &= \oint_{\partial\Omega} \beta(\hat{x}, \hat{y}) B_i(\hat{x}) B_j(\hat{y}) B_k(\hat{x}) B_\ell(\hat{y}) d\hat{x} d\hat{y}, \\ \tilde{Q}_{ijkl} &= \oint_{\partial\Omega} \frac{\rho(\hat{x}, \hat{y})}{v(\hat{x}, \hat{y})} B_i(\hat{x}) B_j(\hat{y}) B_k(\hat{x}) B_\ell(\hat{y}) d\hat{x} d\hat{y}. \end{aligned}$$

By using the expressions of B_i and B_j given in (25) and by introducing the variables $s \in [0, n_1]$ and $\tau \in [0, n_2]$ such that $x = a + sh_1$ and $y = c + \tau h_2$, we obtain

$$D_{ijkl} = \frac{h_2}{h_1} D_1^1(i, k) D_2^0(j, \ell) + \frac{h_1}{h_2} D_1^0(i, k) D_2^1(j, \ell),$$

where the partial coefficients of the matrices D_1^l and D_2^l ($l = 0, 1$) are given by

$$\begin{aligned} D_1^l(i, k) &= \int_0^{n_1} \mathbb{B}_\gamma^{(l)}(s - i + \gamma + 1) \mathbb{B}_\gamma^{(l)}(s - k + \gamma + 1) ds, \\ D_2^l(j, \ell) &= \int_0^{n_2} \mathbb{B}_\gamma^{(l)}(\tau - j + \gamma + 1) \mathbb{B}_\gamma^{(l)}(\tau - \ell + \gamma + 1) d\tau, \end{aligned}$$

with $\mathbb{B}_\gamma^{(l)}$ is the derivative of the normalized uniform spline function of order l , and

$$U_{ijkl} = h_1 h_2 U_1(i, k) U_2(j, \ell),$$

where the partial coefficients of U_1 and U_2 are given by

$$\begin{aligned} U_1(i, k) &= \int_0^{n_1} \frac{1}{v_1^2(a + sh_1)} \mathbb{B}_\gamma(s - i + \gamma + 1) \mathbb{B}_\gamma(s - k + \gamma + 1) ds, \\ U_2(j, \ell) &= \int_0^{n_2} \frac{1}{v_2^2(c + \tau h_2)} \mathbb{B}_\gamma(\tau - j + \gamma + 1) \mathbb{B}_\gamma(\tau - \ell + \gamma + 1) d\tau, \end{aligned}$$

where we have assumed that $v(a + sh_1, \tau h_2) = v_1(a + sh_1) v_2(c + \tau h_2)$. Similarly,

$$\begin{aligned} Q_{ijkl} &= h_2 \Gamma^{(a)}(i, k) \Lambda_a(j, \ell) + h_2 \Gamma^{(b)}(i, k) \Lambda_b(j, \ell) + h_1 \Lambda_c(i, k) \Gamma^{(c)}(j, \ell) + h_1 \Lambda_d(i, k) \Gamma^{(d)}(j, \ell) + \\ &\quad \beta(a, c) \Gamma^{(a)}(i, k) \Gamma^{(c)}(j, \ell) + \beta(a, d) \Gamma^{(a)}(i, k) \Gamma^{(d)}(j, \ell) + \\ &\quad \beta(b, c) \Gamma^{(b)}(i, k) \Gamma^{(c)}(j, \ell) + \beta(b, d) \Gamma^{(b)}(i, k) \Gamma^{(d)}(j, \ell), \end{aligned}$$

and

$$\begin{aligned} \tilde{Q}_{ijkl} &= h_2 \Gamma^{(a)}(i, k) \Upsilon_a(j, \ell) + h_2 \Gamma^{(b)}(i, k) \Upsilon_b(j, \ell) + h_1 \Upsilon_c(i, k) \Gamma^{(c)}(j, \ell) + h_1 \Upsilon_d(i, k) \Gamma^{(d)}(j, \ell) + \\ &\quad \frac{\rho(a, c)}{v(a, c)} \Gamma^{(a)}(i, k) \Gamma^{(c)}(j, \ell) + \frac{\rho(a, d)}{v(a, d)} \Gamma^{(a)}(i, k) \Gamma^{(d)}(j, \ell) + \\ &\quad \frac{\rho(b, d)}{v(a, d)} \Gamma^{(b)}(i, k) \Gamma^{(c)}(j, \ell) + \frac{\rho(b, d)}{v(b, d)} \Gamma^{(b)}(i, k) \Gamma^{(d)}(j, \ell), \end{aligned}$$

where the partial coefficients of \mathbf{Q}_{ijkl} and $\tilde{\mathbf{Q}}_{ijkl}$ are given by

$$\begin{aligned}
\Lambda_c(i, k) &= \int_0^{n_1} \beta(a + sh_1, c) \mathbb{B}_\gamma(s - i + \gamma + 1) \mathbb{B}_\gamma(s - k + \gamma + 1) ds, \\
\Lambda_a(j, \ell) &= \int_0^{n_2} \beta(a, c + \tau h_2) \mathbb{B}_\gamma(\tau - j + \gamma + 1) \mathbb{B}_\gamma(\tau - \ell + \gamma + 1) d\tau, \\
\Lambda_d(i, k) &= \int_0^{n_1} \beta(a + sh_1, d) \mathbb{B}_\gamma(s - i + \gamma + 1) \mathbb{B}_\gamma(s - k + \gamma + 1) ds, \\
\Lambda_b(j, \ell) &= \int_0^{n_2} \beta(b, c + \tau h_2) \mathbb{B}_\gamma(\tau - j + \gamma + 1) \mathbb{B}_\gamma(\tau - \ell + \gamma + 1) d\tau, \\
\Upsilon_c(i, k) &= \int_0^{n_1} \frac{\rho(a + sh_1, c)}{v(a + sh_1, c)} \mathbb{B}_\gamma(s - i + \gamma + 1) \mathbb{B}_\gamma(s - k + \gamma + 1) ds, \\
\Upsilon_a(j, \ell) &= \int_0^{n_2} \frac{\rho(a, c + \tau h_2)}{v(a, c + \tau h_2)} \mathbb{B}_\gamma(\tau - j + \gamma + 1) \mathbb{B}_\gamma(\tau - \ell + \gamma + 1) d\tau, \\
\Upsilon_d(i, k) &= \int_0^{n_1} \frac{\rho(a + sh_1, d)}{v(a + sh_1, d)} \mathbb{B}_\gamma(s - i + \gamma + 1) \mathbb{B}_\gamma(s - k + \gamma + 1) ds, \\
\Upsilon_b(j, \ell) &= \int_0^{n_2} \frac{\rho(b, c + \tau h_2)}{v(b, c + \tau h_2)} \mathbb{B}_\gamma(\tau - j + \gamma + 1) \mathbb{B}_\gamma(\tau - \ell + \gamma + 1) d\tau,
\end{aligned}$$

and

$$\begin{aligned}
\Gamma^{(a)}(i, k) &= \mathbb{B}_\gamma(-i + \gamma + 1) \mathbb{B}_\gamma(-k + \gamma + 1), & \Gamma^{(b)}(i, k) &= \mathbb{B}_\gamma(n_1 - i + \gamma + 1) \mathbb{B}_\gamma(n_1 - k + \gamma + 1), \\
\Gamma^{(c)}(j, \ell) &= \mathbb{B}_\gamma(-j + \gamma + 1) \mathbb{B}_\gamma(-\ell + \gamma + 1), & \Gamma^{(d)}(j, \ell) &= \mathbb{B}_\gamma(n_2 - j + \gamma + 1) \mathbb{B}_\gamma(n_2 - \ell + \gamma + 1),
\end{aligned}$$

for all $\gamma \in \mathbb{N}$. Hence, the weight matrix $\mathbf{A}(\omega)$ is given by

$$\mathbf{A}(\omega) = \mathbf{M}_D + \mathbf{Q}_{\partial\Omega} + i\omega \tilde{\mathbf{Q}}_{\partial\Omega} - \omega^2 \mathbf{M}_U,$$

where the matrices \mathbf{M}_D , \mathbf{M}_U , $\mathbf{Q}_{\partial\Omega}$, and $\tilde{\mathbf{Q}}_{\partial\Omega}$ can be decomposed as a sum of Kronecker products as follows

$$\begin{aligned}
\mathbf{M}_D &= \frac{h_2}{h_1} [D_2^0 \otimes D_1^1]^\top + \frac{h_1}{h_2} [D_2^1 \otimes D_1^0]^\top, \\
\mathbf{M}_U &= h_1 h_2 [U_2 \otimes U_1]^\top, \\
\mathbf{Q}_{\partial\Omega} &= h_1 \left[\Gamma^{(c)} \otimes \Lambda_c + \Gamma^{(d)} \otimes \Lambda_d \right]^\top + h_2 \left(\Lambda_a \otimes \Gamma^{(a)} + \Lambda_b \otimes \Gamma^{(b)} \right)^\top + \\
&\quad \left[\beta(a, d) \Gamma^{(d)} \otimes \Gamma^{(a)} + \beta(b, d) \Gamma^{(d)} \otimes \Gamma^{(b)} \right]^\top + \left[\beta(a, c) \Gamma^{(c)} \otimes \Gamma^{(a)} + \beta(b, c) \Gamma^{(c)} \otimes \Gamma^{(b)} \right]^\top, \\
\tilde{\mathbf{Q}}_{\partial\Omega} &= h_1 \left[\Gamma^{(c)} \otimes \Upsilon_c + \Gamma^{(d)} \otimes \Upsilon_d \right]^\top + h_2 \left[\Upsilon_a \otimes \Gamma^{(a)} + \Upsilon_b \otimes \Gamma^{(b)} \right]^\top + \\
&\quad \left[\frac{\rho(a, d)}{v(a, d)} \Gamma^{(d)} \otimes \Gamma^{(a)} + \frac{\rho(b, d)}{v(b, d)} \Gamma^{(d)} \otimes \Gamma^{(b)} \right]^\top + \left[\frac{\rho(a, c)}{v(a, c)} \Gamma^{(c)} \otimes \Gamma^{(a)} + \frac{\rho(b, c)}{v(b, c)} \Gamma^{(c)} \otimes \Gamma^{(b)} \right]^\top.
\end{aligned}$$

Finally, the coefficients $\mathcal{J}_{h,kl}(\omega) = \mathcal{L}_\omega(B_{kl})$ of the source term matrix are given by

$$\mathcal{J}_{h,kl}(\omega) = \oint_{\partial\Omega} G(\hat{x}, \hat{y}, \omega) B_{kl}(\hat{x}, \hat{y}) d\hat{x} d\hat{y} + \int_c^d \int_a^b F(x, y, \omega) B_{kl}(x, y) dx dy.$$

We also use similar techniques as above to obtain

$$\begin{aligned}
F_{h,kl}(\omega) &= \int_c^d \int_a^b F(x, y, \omega) B_{kl}(x, y) dx dy, \\
&= h_1 h_2 \int_0^{n_2} \int_0^{n_1} F(a + sh_1, c + \tau h_2, \omega) \mathbb{B}_\gamma(s - k + \gamma + 1) \mathbb{B}_\gamma(\tau - \ell + \gamma + 1) ds d\tau,
\end{aligned}$$

and

$$\begin{aligned}
\mathbf{G}_{h,k\ell}(\omega) &= \oint_{\partial\Omega} G(\hat{x}, \hat{y}, \omega) B_{k\ell}(\hat{x}, \hat{y}) d\hat{x}, \hat{y}, \\
&= h_2 \mathbb{B}_\gamma(-k + \gamma + 1) \int_0^{n_2} G(a, c + h_2\tau, \omega) \mathbb{B}_\gamma(\tau - \ell + \gamma + 1) d\tau + \\
&\quad h_2 \mathbb{B}_\gamma(n_1 - k + \gamma + 1) \int_0^{n_2} G(b, c + h_2\tau, \omega) \mathbb{B}_\gamma(\tau - \ell + \gamma + 1) d\tau + \\
&\quad h_1 \mathbb{B}_\gamma(-\ell + \gamma + 1) \int_0^{n_1} G(a + h_1s, c, \omega) \mathbb{B}_\gamma(s - k + \gamma + 1) ds + \\
&\quad h_1 \mathbb{B}_\gamma(n_2 - \ell + \gamma + 1) \int_0^{n_1} G(a + h_1s, d, \omega) \mathbb{B}_\gamma(s - k + \gamma + 1) ds + \\
&\quad \mathbb{B}_\gamma(-\ell + \gamma + 1) \left(G(a, c, \omega) \mathbb{B}_\gamma(-k + \gamma + 1) + G(b, c, \omega) \mathbb{B}_\gamma(n_1 - k + \gamma + 1) \right) + \\
&\quad \mathbb{B}_\gamma(n_2 - \ell + \gamma + 1) \left(G(a, d, \omega) \mathbb{B}_\gamma(-k + \gamma + 1) + G(b, d, \omega) \mathbb{B}_\gamma(n_1 - k + \gamma + 1) \right).
\end{aligned}$$

Hence, for $1 \leq k \leq N_{\gamma,1}$ and $1 \leq \ell \leq N_{\gamma,2}$, the coefficients $\mathcal{J}_{h,k\ell}(\omega)$ are given by

$$\mathcal{J}_{h,k\ell}(\omega) = \mathbf{G}_{h,k\ell}(\omega) + \mathbf{F}_{h,k\ell}(\omega).$$

Thus, by solving the linear system (30) we obtain the vector $z_h(\omega)$ depending on the frequency variable ω , then we evaluate the matrix-valued function $\mathbf{Z}_h(\omega)$ with the coefficients appearing in (28) of the approximate solution $u_h(\cdot, \cdot, \omega)$.

3.3. Solution of the inverse Fourier transform

To reconstruct the time-dependent solution of the transverse electromagnetic wave problem, we proceed by the inverse Fourier transform. Here, an approximation ϕ_h of the solution ϕ_* is obtained as the inverse Fourier transform of u_h . It should be stressed that the Fourier transform and its inverse are considered as Fourier-Plancherel isomorphism between $L^2(\mathbb{R}, dt)$ and $L^2(\mathbb{R}, d\omega)$ and therefore, we have the following result the proof of which can be found in [48]:

Theorem 2. *For every fixed time t , the problem (1)-(3) has a unique solution $\phi_*(\cdot, t)$ belonging to the space $H^1(\Omega)$, which is obtained as the inverse Fourier transform of the unique solution $u_*(\cdot, \omega)$ of the problem (8)-(9) and it is given by*

$$\phi_*(x, y, t) = \frac{1}{\sqrt{2\pi}} \int_{-\infty}^{+\infty} u_*(x, y, \omega) e^{it\omega} d\omega, \quad \forall (x, y) \in \bar{\Omega}. \quad (31)$$

Furthermore, if $u_*(\cdot, \omega) \in \widehat{H}_m(\Omega)$ then, the unique solution $\phi_*(\cdot, t)$ of the wave problem (1)-(3) belongs to the space $H^m(\Omega)$. ■

Hence, an approximate solution $\phi_h(x, y, t)$ of the problem (1)-(3) is obtained by using the inverse Fourier transform in (31) as

$$\phi_h(x, y, t) = \frac{1}{\sqrt{2\pi}} \int_{-\infty}^{+\infty} u_h(x, y, \omega) e^{it\omega} d\omega. \quad (32)$$

Consider the finite-dimensional vector space $\mathbb{V}_h^{(\gamma, m)}$ with the dimension $N_\gamma = N_{\gamma,1}N_{\gamma,2}$ defined as

$$\mathbb{V}_h^{(\gamma, m)} = \left\{ \phi_h(\cdot, t) \in H^m(\Omega) : \phi_h(\cdot, t)|_{\mathcal{C}_{ij}} \in \mathbb{P}_\gamma \otimes \mathbb{P}_\gamma(\Omega); \text{ for } 0 \leq i \leq n_1 - 1, 0 \leq j \leq n_2 - 1 \right\}.$$

Note that for $m = 1$, the approximate solution $\phi_h(\cdot, \cdot, t)$ is an element of the space $\mathbb{V}_h^{(\gamma, 1)}$ and it is given by

$$\phi_h(x, y, t) = \sum_{i=1}^{N_{\gamma,1}} \sum_{j=1}^{N_{\gamma,2}} V_{h,ij}(t) B_{ij}(x, y), \quad (x, y, t) \in \Omega \times [0, T], \quad (33)$$

where the functions

$$V_{h,ij}(t) = \frac{1}{\sqrt{2\pi}} \int_{-\infty}^{+\infty} Z_{h,ij}(\omega) e^{it\omega} d\omega, \quad (34)$$

are the inverse Fourier transforms of the functions $Z_{h,ij}$ given in (28). It should also be noted that when the signal $\phi(\mathbf{x}, \cdot)$ is a fast decay function or it belongs to the Schwartz space $\mathcal{S}(\mathbb{R})$ with respect to the time variable, we use the Gauss-Hermite quadrature to compute the approximate solution ϕ_h of the analytical solution ϕ_* , compare [45, 46]. For every $1 \leq i \leq N_{\gamma,1}$ and $1 \leq j \leq N_{\gamma,2}$, using the definition

$$\varphi_{ij}(\omega, t) = \frac{1}{\sqrt{2\pi}} e^{(\omega^2 + it\omega)} Z_{h,ij}(\omega),$$

we obtain

$$V_{h,ij}(t) = \int_{-\infty}^{+\infty} \varphi_{ij}(\omega, t) e^{-\omega^2} d\omega, \quad 1 \leq i \leq N_{\gamma,1}, \quad 1 \leq j \leq N_{\gamma,2}. \quad (35)$$

Here, to compute the integral in (35), we use the Gauss-Hermite quadrature formula as

$$\int_{-\infty}^{+\infty} \varphi_{ij}(\omega, t) e^{-\omega^2} d\omega \simeq \sum_{\ell=0}^{\tilde{m}} \alpha_{\ell} \varphi_{ij}(\omega_{\ell}, t),$$

where the nodes $(\omega_{\ell})_{0 \leq \ell \leq \tilde{m}}$ are the zeros of the Hermite polynomial $\mathcal{H}_{\tilde{m}+1}$ of degree $\tilde{m} + 1$, and the weight coefficients $(\alpha_{\ell})_{0 \leq \ell \leq \tilde{m}}$ are given by the Christoffel-Darboux formula, see [46] for more details. Thus, the coefficients $V_{h,ij}(t)$ given in (34) are approximated by

$$V_{h,ij}(t) \simeq \sum_{\ell=0}^{\tilde{m}} \alpha_{\ell} \varphi_{ij}(\omega_{\ell}, t), \quad \text{for } 1 \leq i \leq N_{\gamma,1}, \quad 1 \leq j \leq N_{\gamma,2}. \quad (36)$$

Finally, using (33) and (36), we obtain

$$\phi_h(x, y, t) \simeq \sum_{i=1}^{N_{\gamma,1}} \sum_{j=1}^{N_{\gamma,2}} \left(\sum_{\ell=0}^{\tilde{m}} \alpha_{\ell} \varphi_{ij}(\omega_{\ell}, t) \right) B_{ij}(x, y) = \sum_{\ell=0}^{\tilde{m}} \alpha_{\ell} \left(\sum_{i=1}^{N_{\gamma,1}} \sum_{j=1}^{N_{\gamma,2}} \varphi_{ij}(\omega_{\ell}, t) B_{ij}(x, y) \right).$$

It should be stressed that for functions which are not in the Schwartz space $\mathcal{S}(\mathbb{R})$ with respect to the time variable, we compute the coefficients $V_{h,ij}(t)$ using other quadrature methods such as Left-rectangle, Right-rectangle, Gauss-Legendre, Trapezoidal, Simpson, and Newton-Cotes quadratures among others. For instance, assuming that $f_c = \frac{\omega_{\max}}{2}$ is the Nyquist critical frequency where $\omega_{\max} = \frac{m}{T}$, we discretize the interval $[-f_c, f_c]$ using equally spaced knots $\omega_k = -f_c + k \Delta\omega$, $k = 0, 1, 2, \dots, m$, with $\omega_0 = -f_c$, $\omega_m = f_c$ and $\Delta\omega = \frac{1}{T}$. To compute numerically the function $V_{h,ij}(t)$, we use the following approach

$$V_{h,ij}(t) = \frac{1}{\sqrt{2\pi}} \int_{-\infty}^{+\infty} Z_{h,ij}(\omega) e^{it\omega} d\omega \simeq \frac{1}{\sqrt{2\pi}} \int_{-f_c}^{f_c} Z_{h,ij}(\omega) e^{it\omega} d\omega. \quad (37)$$

Needless to mention that to solve the problem of functions which have a very oscillating structure and to obtain a sufficiently precise approximate value of the inverse Fourier transform integral, it is essential to provide a very large number m of the quadrature points. In our simulations carried out in the present study, the number of the quadrature points does not exceed $m = 40$ for all considered wave regimes.

4. Convergence analysis and error estimates

In this section we establish relevant results on the error estimates for the proposed spline finite element method. Again, the domain is assumed $\Omega = [a, b] \times [c, d]$ covered with the mesh Ω_h defined in (24) and we consider the subspace $\widehat{\mathbb{S}}_h^{(\gamma, m)}(\Omega)$ of $\widehat{\mathcal{V}}_h^{(\gamma, m)}$ defined as

$$\widehat{\mathbb{S}}_h^{(\gamma, m)}(\Omega) = \left\{ u_h \in \mathcal{C}^m(\overline{\Omega}) : u_h \Big|_{\mathcal{C}_{ij}} \in \mathbb{P}_\gamma \otimes \mathbb{P}_\gamma(\Omega), \quad \text{for } 0 \leq i \leq n_1 - 1, 0 \leq j \leq n_2 - 1 \right\}.$$

We consider the B -spline spaces $\widehat{\mathbb{S}}_{h_1}^{(\gamma, m)}([a, b])$ and $\widehat{\mathbb{S}}_{h_2}^{(\gamma, m)}([c, d])$ defined as in [45, 46]. For each spatial step h , we consider the interpolating operator $\mathcal{I}_h^{(\gamma, m)} : \widehat{\mathbb{H}}_m \rightarrow \widehat{\mathbb{S}}_h^{(\gamma, m)}(\Omega)$ such that for all $u \in \widehat{\mathbb{H}}_m$, the function $\mathcal{I}_h^{(\gamma, m)} u$ is the unique spline in the tensorial space $\widehat{\mathbb{S}}_h^{(\gamma, m)}(\Omega) = \widehat{\mathbb{S}}_{h_1}^{(\gamma, m)}([a, b]) \otimes \widehat{\mathbb{S}}_{h_2}^{(\gamma, m)}([c, d])$ given by

$$\mathcal{I}_h^{(\gamma, m)} u(x, y) = \sum_{j=1}^{N_{\gamma, 1}} \sum_{i=1}^{N_{\gamma, 2}} \delta_{ij}^{(m)} B_{ij}(x, y), \quad \forall (x, y) \in \overline{\Omega}, \quad (38)$$

and satisfying the following interpolating conditions

$$\mathcal{I}_h^{(\gamma, m)} u(x_i, y_j) = u(x_i, y_j), \quad (39a)$$

$$\frac{\partial^\ell (\mathcal{I}_h^{(\gamma, m)} u)}{\partial x^\ell}(\hat{x}, y_j) = \frac{\partial^\ell u}{\partial x^\ell}(\hat{x}, y_j), \quad \text{and} \quad \frac{\partial^\ell (\mathcal{I}_h^{(\gamma, m)} u)}{\partial y^\ell}(x_i, \hat{y}) = \frac{\partial^\ell u}{\partial y^\ell}(x_i, \hat{y}), \quad (39b)$$

$$\frac{\partial^{\ell_1 + \ell_2} (\mathcal{I}_h^{(\gamma, m)} u)}{\partial x^{\ell_1} \partial y^{\ell_2}}(\hat{x}, \hat{y}) = \frac{\partial^{\ell_1 + \ell_2} u}{\partial x^{\ell_1} \partial y^{\ell_2}}(\hat{x}, \hat{y}), \quad \ell_1 + \ell_2 = 1, 2, \dots, m - 1. \quad (39c)$$

for $i = 0, 1, \dots, n_1, j = 0, 1, \dots, n_2, \ell = 1, 2, \dots, m - 1$ and $(\hat{x}, \hat{y}) \in \{a, b\} \times \{c, d\}$. Note that the coefficients $\delta_{ij}^{(m)}$ in (38) are computed using the interpolating conditions given by (39). By setting $\boldsymbol{\delta}$ the vector with entries $\delta_{ij}^{(m)}$ and \mathbf{u} the vector with entries given in the right-hand sides of (39), the conditions (39) lead to the following linear system

$$(\mathbf{P}_2 \otimes \mathbf{P}_1) \boldsymbol{\delta} = \mathbf{u}, \quad (40)$$

where \mathbf{P}_1 and \mathbf{P}_2 are the matrices obtained by using the conditions (39), see [45] for more details. Next, we state the following error estimates:

Lemma 2. *Let u be a generic function in $\widehat{\mathbb{H}}_2$. Then, there exist constants $c_1 > 0$ and $c_2 > 0$ such that*

- a) $\left\| \Delta u - \Delta(\mathcal{I}_h^{(\gamma, 2)} u) \right\|_{\widehat{\mathbb{L}}_2} \leq \|u\|_{\widehat{\mathbb{H}}_2},$
- b) $\left\| \nabla u - \nabla(\mathcal{I}_h^{(\gamma, 2)} u) \right\|_{\widehat{\mathbb{L}}_2} \leq c_1 h \|u\|_{\widehat{\mathbb{H}}_2},$
- c) $\left\| u - \mathcal{I}_h^{(\gamma, 2)} u \right\|_{\widehat{\mathbb{L}}_2} \leq c_2 h^2 \|u\|_{\widehat{\mathbb{H}}_2}. \quad \square$

PROOF. From the results reported in [54, 46, 55, 56] for the one-dimensional case, it is easy to realize that, for $u \in \mathcal{C}^2(\Omega)$, we have

$$\begin{aligned} \left\| \frac{\partial^2 u}{\partial x^2}(\cdot, y) - \frac{\partial^2 (\mathcal{I}_h^{(\gamma, 2)} u)}{\partial x^2}(\cdot, y) \right\|_{\widehat{\mathbb{L}}_2} &\leq \left\| \frac{\partial^2 u}{\partial x^2}(\cdot, y) \right\|_{\widehat{\mathbb{L}}_2}, \\ \left\| \frac{\partial u}{\partial x}(\cdot, y) - \frac{\partial (\mathcal{I}_h^{(\gamma, 2)} u)}{\partial x}(\cdot, y) \right\|_{\widehat{\mathbb{L}}_2} &\leq \frac{2h_1}{\pi} \left\| \frac{\partial^2 u}{\partial x^2}(\cdot, y) \right\|_{\widehat{\mathbb{L}}_2}, \\ \left\| u(\cdot, y) - \mathcal{I}_h^{(\gamma, 2)} u(\cdot, y) \right\|_{\widehat{\mathbb{L}}_2} &\leq \frac{2h_1^2}{\pi^2} \left\| \frac{\partial^2 u}{\partial x^2}(\cdot, y) \right\|_{\widehat{\mathbb{L}}_2}, \end{aligned}$$

and similarly,

$$\begin{aligned} \left\| \frac{\partial^2 u}{\partial y^2}(x, \cdot) - \frac{\partial^2 (\mathcal{I}_h^{(\gamma, 2)} u)}{\partial y^2}(x, \cdot) \right\|_{\widehat{L}_2} &\leq \left\| \frac{\partial^2 u}{\partial y^2}(x, \cdot) \right\|_{\widehat{L}_2}, \\ \left\| \frac{\partial u}{\partial y}(x, \cdot) - \frac{\partial (\mathcal{I}_h^{(\gamma, 2)} u)}{\partial y}(x, \cdot) \right\|_{\widehat{L}_2} &\leq \frac{2h_2}{\pi} \left\| \frac{\partial^2 u}{\partial y^2}(x, \cdot) \right\|_{\widehat{L}_2}, \\ \left\| u(x, \cdot) - \mathcal{I}_h^{(\gamma, 2)} u(x, \cdot) \right\|_{\widehat{L}_2} &\leq \frac{2h_2^2}{\pi^2} \left\| \frac{\partial^2 u}{\partial y^2}(x, \cdot) \right\|_{\widehat{L}_2}. \end{aligned}$$

Hence, the estimates in a), b) and c) are obtained from the triangular inequality. \blacksquare

We also recall the following result which is a direct consequence of the Céa lemma in [57]:

Lemma 3. *For a fixed frequency $\omega \in \mathbb{R}$, if $u(\cdot, \omega)$ (resp. $u_h(\cdot, \omega)$) is a solution of the variational problem (10) (resp. (27)), then*

$$\|u(\cdot, \omega) - u_h(\cdot, \omega)\|_{\widehat{H}_m} \leq \frac{M_3}{\alpha} (1 + \omega^2) \inf_{v_h \in \widehat{\mathcal{V}}_h^{(\gamma, m)}} \|u(\cdot, \omega) - v_h(\cdot, \omega)\|_{\widehat{H}_m},$$

where M_3 and α are respectively, the constants related to the continuity and the coercivity of \mathcal{A}_ω and are given in (15) and (16), respectively. \blacksquare

Next, we establish the following error estimates for the numerical solutions in the appropriate norms:

Theorem 3. *Assume that the functions $v \in \mathcal{C}(\overline{\Omega})$, $f \in \mathbf{H}^2(\mathbb{R}; \mathbf{L}_2)$ and $g \in \mathbf{H}^2(\mathbb{R}, \mathbf{L}^2(\partial\Omega))$. Then, we have the following results:*

- (1) *The function $\nabla^2 \phi_* \in \mathbf{L}^2(\mathbb{R}; \mathbf{L}_2)$ or $\phi_* \in \mathbf{L}^2(\mathbb{R}; \mathbf{H}_2)$.*
- (2) *There exists a constant $\widetilde{C} > 0$ such that*

$$\|u_* - u_{*h}\|_{\mathbf{L}^2(\mathbb{R}; \widehat{L}_2)} \leq \widetilde{C} h^2 (1 + h^2)^{1/2} \|\phi_*\|_{\mathbf{H}^2(\mathbb{R}; \mathbf{H}_2)},$$

and

$$\|u_* - u_{*h}\|_{\mathbf{L}^2(\mathbb{R}; \widehat{H}_1)} \leq \widetilde{C} h (1 + h^2)^{1/2} \|\phi_*\|_{\mathbf{H}^2(\mathbb{R}; \mathbf{H}_2)}.$$

- (3) *The convergence order is*

$$\|\phi_* - \phi_h\|_{\mathbf{L}^2(\mathbb{R}; \mathbf{L}_2)} = \mathcal{O}(h^2), \quad \text{and} \quad \|\phi_* - \phi_h\|_{\mathbf{L}^2(\mathbb{R}; \mathbf{H}_1)} = \mathcal{O}(h). \quad \square$$

PROOF.

- (1) Here, we have $u_* = \widehat{\phi}_*$. Since $F(\cdot, \omega) \in \widehat{L}_2$ and $u_*(\cdot, \omega) \in \widehat{H}_1$, we deduce from the following relation

$$\nabla^2 u_*(\mathbf{x}, \omega) = -F(\mathbf{x}, \omega) - \frac{\omega^2}{v^2(\mathbf{x})} u_*(\mathbf{x}, \omega),$$

that $\nabla^2 u_*(\cdot, \omega)$ belongs to \widehat{L}_2 . Next, using the inequality $(|a| + |b|)^2 \leq 4(|a|^2 + |b|^2)$ it follows that there exists a constant $M_4 > 0$ such that

$$\left| \nabla^2 \widehat{\phi}_*(\mathbf{x}, \omega) \right|^2 \leq \frac{M_4 (1 + \omega^2)^2}{\alpha^2} \left(|F(\mathbf{x}, \omega)|^2 + |u_*(\mathbf{x}, \omega)|^2 \right),$$

for all $\mathbf{x} \in \bar{\Omega}$. The Lebesgue theorem for derivatives under the integral sign allows us to write $\nabla^2 \widehat{\phi}_*(\cdot, \omega) = \widehat{\nabla^2 \phi}_*(\cdot, \omega)$. By integrating over Ω in the last inequality, we obtain

$$\left\| \widehat{\nabla^2 \phi}_*(\cdot, \omega) \right\|_{\widehat{L}_2}^2 \leq \frac{M_4(1+\omega^2)^2}{\alpha^2} \left(\|F(\cdot, \omega)\|_{L_2}^2 + \|u_*(\cdot, \omega)\|_{\widehat{H}_1}^2 \right).$$

From Theorem 1, we have $\|u_*(\cdot, \omega)\|_{\widehat{H}_1} \leq \frac{\mathcal{R}(\omega)}{\alpha}$ where $\mathcal{R}(\omega)$ is given in (14). It follows that, there exists a constant $M_5 > 0$ such that

$$\left\| \nabla^2 \widehat{\phi}_*(\cdot, \omega) \right\|_{\widehat{L}_2}^2 \leq \frac{M_5(1+\omega^2)^2}{\alpha^4} \left(\|\widehat{f}(\cdot, \omega)\|_{L_2}^2 + \|\widehat{g}(\cdot, \omega)\|_{L^2(\partial\Omega)}^2 \right).$$

Integrating over \mathbb{R} with respect to ω taking into account the considered assumptions on f and g , we obtain

$$\|\nabla^2 \phi_*\|_{L^2(\mathbb{R}; L_2)}^2 \leq \frac{M_5}{\alpha^4} \left(\|f\|_{H^2(\mathbb{R}; L_2)}^2 + \|g\|_{H^2(\mathbb{R}; L^2(\partial\Omega))}^2 \right) < \infty.$$

(2) The following error bound is obtained by using Lemma 3. Thus, we have

$$\|u_*(\cdot, \omega) - u_{*h}(\cdot, \omega)\|_{\widehat{L}_2} \leq \frac{M_3}{\alpha} (1+\omega^2) \inf_{v_h \in \widehat{\mathcal{V}}_h^{(\gamma, 2)}} \|u_*(\cdot, \omega) - v_h(\cdot, \omega)\|_{\widehat{L}_2}, \quad (41)$$

where M_3 and α are the continuity and the coercivity constants given in (15) and (16), respectively. Since $\mathcal{I}_h^{(\gamma, 2)} u_*(\cdot, \omega)$ belongs to $\widehat{\mathcal{S}}_h^{(\gamma, 2)} \subset \widehat{\mathcal{V}}_h^{(\gamma, 2)}$, it follows that

$$\inf_{v_h \in \widehat{\mathcal{V}}_h^{(\gamma, 2)}} \|u_*(\cdot, \omega) - v_h(\cdot, \omega)\|_{\widehat{L}_2} \leq \left\| u_*(\cdot, \omega) - \mathcal{I}_h^{(\gamma, 2)} u_*(\cdot, \omega) \right\|_{\widehat{L}_2}. \quad (42)$$

Since the solution $u_*(\cdot, \omega)$ belongs to \widehat{H}_2 according to Lemma 2, we obtain

$$\left\| u_*(\cdot, \omega) - \mathcal{I}_h^{(\gamma, 2)} u_*(\cdot, \omega) \right\|_{\widehat{L}_2} \leq c_1 h^2 \|u_*(\cdot, \omega)\|_{\widehat{H}_2}, \quad (43)$$

and

$$\left\| \nabla u_*(\cdot, \omega) - \nabla(\mathcal{I}_h^{(\gamma, 2)} u_*)(\cdot, \omega) \right\|_{\widehat{L}_2} \leq c_2 h \|u_*(\cdot, \omega)\|_{\widehat{H}_2}. \quad (44)$$

Therefore,

$$\|u_*(\cdot, \omega) - \mathcal{I}_h^{(\gamma, 2)} u_*(\cdot, \omega)\|_{\widehat{H}_1} \leq \sup(c_1, c_2) h (1+h^2)^{\frac{1}{2}} \|u_*(\cdot, \omega)\|_{\widehat{H}_2}. \quad (45)$$

Using the inequalities (41), (42), (44) and (45) along with $\frac{\partial^2 u_*}{\partial x^2}(\cdot, \omega) = \frac{\partial^2 \widehat{\phi}_*}{\partial x^2}(\cdot, \omega)$ and $\frac{\partial^2 u_*}{\partial y^2}(\cdot, \omega) = \frac{\partial^2 \widehat{\phi}_*}{\partial y^2}(\cdot, \omega)$, we obtain the error estimate

$$\|u_*(\cdot, \omega) - u_h(\cdot, \omega)\|_{\widehat{H}_1}^2 \leq \left(\frac{M_3}{\alpha} \right)^2 h^2 (1+h^2) (1+\omega^2)^2 \left\| \widehat{\phi}_*(\cdot, \omega) \right\|_{\widehat{H}_2}^2.$$

Again, integrating over \mathbb{R} with respect to the frequency variable ω , we obtain

$$\|u_* - u_h\|_{L^2(\mathbb{R}; \widehat{H}_1)} \leq \widetilde{C} h \sqrt{1+h^2} \left\| \phi_* \right\|_{H^2(\mathbb{R}; H_2)},$$

with $\widetilde{C} = \frac{M_3}{\alpha}$.

(3) Now, using the Parseval identity it yields

$$\int_{-\infty}^{+\infty} |\phi_*(\mathbf{x}, t) - \phi_h(\mathbf{x}, t)|^2 dt = \frac{1}{2\pi} \int_{-\infty}^{+\infty} |u_*(\mathbf{x}, \omega) - u_h(\mathbf{x}, \omega)|^2 d\omega, \quad (46)$$

and

$$\int_{-\infty}^{+\infty} |\nabla(\phi_* - \phi_h)(\mathbf{x}, t)|^2 dt = \frac{1}{2\pi} \int_{-\infty}^{+\infty} \left| \widehat{\nabla\phi_*}(\mathbf{x}, \omega) - \widehat{\nabla\phi_h}(\mathbf{x}, \omega) \right|^2 d\omega.$$

Therefore, using the Lebesgue theorem of derivation under the integral sign, we obtain

$$\begin{aligned} \int_{-\infty}^{+\infty} |\nabla(\phi_* - \phi_h)(\mathbf{x}, t)|^2 dt &= \frac{1}{2\pi} \int_{-\infty}^{+\infty} \left| \nabla\widehat{\phi_*}(\mathbf{x}, \omega) - \nabla\widehat{\phi_h}(\mathbf{x}, \omega) \right|^2 d\omega, \\ &= \frac{1}{2\pi} \int_{-\infty}^{+\infty} |\nabla u_*(\mathbf{x}, \omega) - \nabla u_h(\mathbf{x}, \omega)|^2 d\omega. \end{aligned} \quad (47)$$

Integrating (46) and (47) over Ω with respect to the variable \mathbf{x} and using the well-established Fubini's theorem, we obtain

$$\int_{-\infty}^{+\infty} \|\phi_*(\cdot, t) - \phi_h(\cdot, t)\|_{\widehat{H}_1}^2 dt = \frac{1}{2\pi} \int_{-\infty}^{+\infty} \|u_*(\cdot, \omega) - u_h(\cdot, \omega)\|_{\widehat{H}_1}^2 d\omega.$$

Then,

$$\|\phi_* - \phi_h\|_{L^2(\mathbb{R}; L_2)} = \frac{1}{\sqrt{2\pi}} \|u_* - u_h\|_{L^2(\mathbb{R}; \widehat{L}_2)} \quad \text{or} \quad \|\phi_* - \phi_h\|_{L^2(\mathbb{R}; H_1)} = \frac{1}{\sqrt{2\pi}} \|u_* - u_h\|_{L^2(\mathbb{R}; \widehat{H}_1)}.$$

Hence, using the result (2) in Theorem 3, we obtain the following error estimates

$$\|\phi_* - \phi_h\|_{L^2(\mathbb{R}; L_2)} \leq \frac{\widetilde{C}}{\sqrt{2\pi}} h^2 \sqrt{1+h^2} \|\phi_*\|_{H^2(\mathbb{R}; H_2)},$$

or

$$\|\phi_* - \phi_h\|_{L^2(\mathbb{R}; H_1)} \leq \frac{\widetilde{C}}{\sqrt{2\pi}} h \sqrt{1+h^2} \|\phi_*\|_{H^2(\mathbb{R}; H_2)},$$

which concludes the proof. \blacksquare

The following result is a direct consequence of Theorem 3 and therefore the proof is omitted:

Theorem 4. *Assume that the functions $v \in \mathcal{C}(\overline{\Omega})$, $f \in L^2(\mathbb{R}; L_2)$ and $g \in L^2(\mathbb{R}, L^2(\partial\Omega))$. Then, the solution ϕ_* of the problem (1)-(3) satisfies*

- $\nabla^2 \phi_* \in H^{-2}(\mathbb{R}; L_2)$.
- There exists a constant $\widetilde{C} > 0$ such that

$$\|\phi_* - \phi_{*h}\|_{H^{-2}(\mathbb{R}; \widehat{H}_1)} \leq \widetilde{C} h(1+h^2)^{1/2} \|\phi_*\|_{L^2(\mathbb{R}; H_2)}. \quad \blacksquare$$

In the following results, a general estimation of the error and convergence order is stated and the proof is reported in [54]:

Lemma 4. *Let $u \in \widehat{H}_m$ and denote by $\partial^\ell u = \frac{\partial^\ell u}{\partial x^{\ell_1} \partial y^{\ell_2}}$ the weak derivatives of u with order $0 \leq \ell = \ell_1 + \ell_2 \leq m$, then $\partial^\ell u \in \widehat{H}_{m-\ell}$ and there exists a positive constant c independent of h such that*

$$\left\| u - (\mathcal{I}_h^{(\gamma, m)} u)^{(\ell)} \right\|_{\widehat{L}_2} \leq c \|h\|_\infty^{m-\ell} \left\| u^{(m)} \right\|_{\widehat{L}_2}, \quad (48)$$

and

$$\left\| u - (\mathcal{I}_h^{(\gamma, m)} u) \right\|_{\widehat{H}_\ell} \leq c \|h\|_\infty^{m-\ell} \|u\|_{\widehat{H}_m}, \quad 0 \leq \ell \leq m. \quad \blacksquare \quad (49)$$

Finally, using the arguments in Lemma 4 and the results of Theorem 3, we obtain the following results for the convergence order:

Theorem 5. *Assume that the solution $\phi_*(\cdot, t)$ is in $H_{\gamma+1}$, then*

- $\phi_* \in L^2(\mathbb{R}; H_{\gamma+1})$.

- *The convergence order is*

$$\|\phi_* - \phi_h\|_{L^2(\mathbb{R}; L_2 \times L_2)} = \mathcal{O}(h^{\gamma+1}). \quad (50)$$

For completeness, the high-order spline finite element method proposed in the present study for the electromagnetic wave problem (1)-(3) is carried out in the steps described in Algorithm 1. In all our computations carried out in this section, the resulting linear system of algebraic equations (30) is decomposed into an LUL^T factorization, then the solution is reduced to backward/forward substitutions after updating the global matrix $\mathbf{A}(\omega)$ and the right-hand side vector $\mathbf{b}_h(\omega)$ for every frequency ω .

5. Numerical results and examples

In this section we assess the performance of the proposed spline finite element method for solving several examples of time-dependent electromagnetic waves. In all our simulations, unless stated otherwise, we solve the equations (1)-(3) in a squared domain $\Omega = [a, b] \times [a, b]$ uniformly discretized using $h_k = \frac{b-a}{n_k}$ with different mesh densities n_k and spline orders γ . For problems with known exact solutions, we compute the L^2 -error between the numerical and analytical solutions as

$$E(h_k) = \frac{\|\phi_e - \phi_{h_k}\|_{L^2}}{\|\phi_e\|_{L^2}},$$

where ϕ_e and ϕ_{h_k} are respectively the exact and numerical solutions of the wave problem (1)-(3). Hence, we calculate the rate of convergence between two consecutive discretizations with h_{k+1} and h_k by

$$\text{Rate} = \frac{\log\left(\frac{E(h_{k+1})}{E(h_k)}\right)}{\log\left(\frac{h_{k+1}}{h_k}\right)}.$$

The above L^2 -error and convergence rates are used to assess the accuracy of the proposed method whereas CPU times are used to evaluate its efficiency for the problems considered in the present study. All the computations are performed on an Intel(R) Core (TM) i7 PC with processor of 12288MB of RAM and 2.6 GHz. The algorithm is implemented in MATLAB and it takes the default optimization of the machine, *i.e.* it is not a parallel code.

5.1. A Gaussian time-dependent wave problem

In this example, we consider the transverse electromagnetic wave problem (1)-(3) with constant wave speed $v = 3000$, $\rho = 5$ and $\beta = 9$. The source term f , the boundary function g , and the initial data ϕ_0 and ϕ_1 are calculated such that the analytical solution of the problem (1)-(3) is given by

$$\phi_e(x, y, t) = A_0 e^{i(\kappa x \cos(\alpha) + \kappa y \sin(\alpha) + \varphi) - \sigma t^2}.$$

Here, we evaluate the accuracy of the frequency-domain method for this example by quantifying the L^2 -error in the real and imaginary parts of the obtained solutions at time $t = 1$ using different mesh densities and \mathbb{B}_γ -spline orders. In all our computations $\sigma = \frac{1}{2}$, $\alpha = \frac{\pi}{4}$, $\varphi = \frac{\pi}{3}$, $\kappa = 2\pi$ and $A_0 = 1$.

Algorithm 1 High-order spline finite element method for frequency-domain problems.

- 1: **Forward stage:** Generate the Fourier transforms $u(\cdot, \omega) = \widehat{\phi}(\cdot, \omega)$, $F(x, y, \omega) = \widehat{f}(x, y, \omega)$, $G(\hat{x}, \hat{y}, \omega) = \widehat{g}(\hat{x}, \hat{y}, \omega)$ of $\phi(x, y, \cdot)$, $f(x, y, \cdot)$ and $g(\hat{x}, \hat{y}, \cdot)$ according to (6).
- 2: **for** each frequency ω **do**
- 3: • Sample the basis functions B_{ij} using the \mathbb{B}_γ -spline as

$$B_{ij}(x, y) = \mathbb{B}_\gamma\left(\frac{x - x_{i-\gamma-1}}{h_1}\right) \mathbb{B}_\gamma\left(\frac{y - y_{j-\gamma-1}}{h_2}\right).$$

- 4: • Construct the approximate solution by

$$u_h(x, y, \omega) = \sum_{i=1}^{N_{\gamma,1}} \sum_{j=1}^{N_{\gamma,2}} Z_{h,ij}(\omega) B_{ij}(x, y).$$

- 5: • Assemble the weak variational formulation into

$$\sum_{i=1}^{N_{\gamma,1}} \sum_{j=1}^{N_{\gamma,2}} Z_{h,ij}(\omega) \mathcal{A}_\omega(B_{ij}, B_{k\ell}) = \mathcal{J}_\omega(B_{k\ell}), \quad k = 1, \dots, N_{\gamma,1}, \quad \ell = 1, \dots, N_{\gamma,2}.$$

- 6: • Solve the linear system

$$\mathbf{A}(\omega) \mathbf{z}_h(\omega) = \mathbf{b}_h(\omega).$$

7: **end for**

- 8: **Backward stage:** Using the inverse Fourier transform (32) and the quadrature methods (3.3)-(37), calculate the coefficients $v_{h,ij}(t)$ ($i = 1, \dots, N_{\gamma,1}, j = 1, \dots, N_{\gamma,2}$) of the vector $v_h(t)$ and reconstruct its corresponding matrix $V_h(t)$.
- 9: • Form the \mathbb{B}_γ -spline basis $B_{ij}(x, y)$ such that

$$u_h(x, y, \omega) = \sum_{i=1}^{N_{\gamma,1}} \sum_{j=1}^{N_{\gamma,2}} Z_{h,ij}(\omega) B_{ij}(x, y).$$

- 10: • For a fixed time $t \in [0, T]$, compute the solution as

$$\phi_h(x, y, t) = \sum_{i=1}^{N_{\gamma,1}} \sum_{j=1}^{N_{\gamma,2}} V_{h,ij}(t) B_{ij}(x, y).$$

The purpose of this example is to compare the performance of the frequency-domain method combined with three different quadrature methods namely, the Right-rectangle quadrature, the Gauss-Hermite quadrature and the Gauss-Legendre quadrature. To this end we summarize in Table 1 values of the L^2 -error and CPU time obtained using each quadrature using meshes with different densities and different \mathbb{B}_γ -spline orders. It is clear that increasing the number of gridpoints for a fixed \mathbb{B}_γ -spline order results in a decrease of the L^2 -error for all considered quadratures. This behavior is also achieved by increasing the \mathbb{B}_γ -spline order for a fixed mesh. The expected order of convergence is also attained for each value of γ in the considered quadratures which confirms the theoretical error estimates for the proposed method. For this example, although there is no significant difference between the errors obtained using the three considered quadratures, there are differences in the computational cost referred to by the CPU time in Table 1. It is evident that increasing the \mathbb{B}_γ -spline order in each method results in a rise in the computational cost. However, on a fixed mesh and for a fixed \mathbb{B}_γ -spline order, the CPU time remains comparable across all considered quadrature schemes. Here, the Right-rectangle quadrature proves to be superior to the other quadrature methods in

Table 1: Convergence results for the example of Gaussian time-dependent wave problem using the considered quadratures with different \mathbb{B}_γ -spline orders and mesh densities. The CPU times are given in seconds.

$\Omega = [0, 1] \times [0, 1]$ and $\gamma = 3$									
n_k	Right-rectangle quadrature			Gauss-Legendre quadrature			Gauss-Hermite quadrature		
	L^2 -error	Rate	CPU	L^2 -error	Rate	CPU	L^2 -error	Rate	CPU
$n_1 = 8$	9.3544E-05	—	1.19	9.2913E-05	—	1.47	9.3563E-05	—	1.44
$n_2 = 16$	5.4251E-06	4.1079	2.97	5.3498E-06	4.1183	4.09	5.4253E-06	4.1082	3.39
$n_3 = 32$	3.3294E-07	4.0263	9.38	3.4636E-07	4.0062	25.7	3.3300E-07	4.0261	24.8
$n_4 = 64$	2.0138E-08	4.0473	85.5	2.0131E-08	4.0484	766	2.0126E-08	4.0473	754
$\Omega = [0, 2] \times [0, 2]$ and $\gamma = 6$									
n_k	Right-rectangle quadrature			Gauss-Legendre quadrature			Gauss-Hermite quadrature		
	L^2 -error	Rate	CPU	L^2 -error	Rate	CPU	L^2 -error	Rate	CPU
$n_1 = 4$	2.4673E-03	—	4.49	2.4673E-03	—	8.45	2.4673E-03	—	5.1
$n_2 = 8$	1.8484E-05	7.0605	6.55	1.8484E-05	7.0605	13.5	1.8484E-05	7.0605	9.06
$n_3 = 16$	7.9395E-08	7.8630	12.8	7.9400E-08	7.8629	31	7.9395E-08	7.8630	22.9
$n_4 = 32$	4.7750E-10	7.3774	58.4	4.7747E-10	7.3776	188	4.7753E-10	7.3773	136
$\Omega = [0, 5] \times [0, 5]$ and $\gamma = 9$									
n_k	Right-rectangle quadrature			Gauss-Legendre quadrature			Gauss-Hermite quadrature		
	L^2 -error	Rate	CPU	L^2 -error	Rate	CPU	L^2 -error	Rate	CPU
$n_1 = 4$	1.9931E-01	—	4.12	2.0250E-01	—	24.7	2.0123E-01	—	5.32
$n_2 = 8$	1.1849E-02	4.0722	8.31	1.1849E-02	4.0951	66.5	1.1849E-02	4.0860	11.2
$n_3 = 16$	2.9414E-06	10.7960	17.8	2.9413E-06	10.0735	200	2.9417E-06	9.8592	29.6
$n_4 = 32$	6.4739E-09	10.0070	132	7.6469E-09	10.4899	2100	8.9097E-09	10.4837	1235

terms of computational efficiency, owing to its simplicity and cost. These findings suggest proceeding for the remaining examples using the Right-rectangle quadrature for investigating the convergence rates of the proposed spline finite element method.

5.2. A time-Reicker wavelet problem

For this example, we consider the well-established time-dependent Reicker wavelet defined by

$$S_\ell(t) = \left(1 - 2\pi^2 \left(t - t_s^{(\ell)}\right)^2 f_{s,\ell}^2\right) e^{-\pi^2 \left(t - t_s^{(\ell)}\right)^2 f_{s,\ell}^2}, \quad \ell = 1, 2,$$

where $f_{s,\ell}$ is the peak frequency and $t_s^{(\ell)}$ is the temporal delay to ensure zero initial conditions, see for example [15]. Thus, for this example we solve the transverse electromagnetic wave problem (1)-(3) in a squared domain Ω for which the source term f , the boundary function g and the initial data ϕ_0 and ϕ_1 are calculated such that the exact solution of the problem is given by

$$\phi_e(t, x, y) = A_0 (S_1(t) + iS_2(t)) e^{i(\mathbf{k} \cdot \mathbf{r} + \varphi)},$$

Table 2: Convergence results for the example of time-Reicker wavelet problem using different \mathbb{B}_γ -spline orders and mesh densities.

$\Omega = [-1, 1] \times [-1, 1]$						
n_k	$\gamma = 1$		$\gamma = 2$		$\gamma = 3$	
	L^2 -error	Rate	L^2 -error	Rate	L^2 -error	Rate
$n_1 = 8$	4.804988E-02	—	2.494675E-03	—	2.654044E-04	—
$n_2 = 16$	1.204180E-02	1.99	2.729276E-04	3.19	1.456931E-05	4.18
$n_3 = 32$	3.010910E-03	1.99	3.249863E-05	3.07	8.802186E-07	4.04
$n_4 = 64$	7.521427E-04	2.00	3.984538E-06	3.02	5.644790E-08	4.00

$\Omega = [-2, 2] \times [-2, 2]$						
n_k	$\gamma = 4$		$\gamma = 5$		$\gamma = 6$	
	L^2 -error	Rate	L^2 -error	Rate	L^2 -error	Rate
$n_1 = 4$	1.00310535E-01	—	4.08010428E-02	—	1.49414712E-02	—
$n_2 = 8$	1.90669413E-03	5.71	5.31512521E-04	6.26	1.47776131E-04	6.65
$n_3 = 16$	3.35308819E-05	5.82	4.14442807E-06	7.00	5.08842758E-07	8.18
$n_4 = 32$	8.83301305E-07	5.24	6.40533626E-08	6.01	2.90775698E-09	7.45

$\Omega = [-4.5, 4.5] \times [-4.5, 4.5]$						
n_k	$\gamma = 7$		$\gamma = 8$		$\gamma = 9$	
	L^2 -error	Rate	L^2 -error	Rate	L^2 -error	Rate
$n_1 = 8$	1.64122226E-01	—	9.67347080E-02	—	4.99224187E-02	—
$n_2 = 16$	1.58621941E-04	10.01	5.29572095E-05	10.83	1.64385368E-05	11.56
$n_3 = 32$	6.10377451E-07	8.02	9.77151478E-08	9.08	1.50147647E-08	10.09

where the phase angle $\varphi \in [0, \pi]$, the wavelength vector $\mathbf{k} = (\kappa \cos(\theta), \kappa \sin(\theta))^T$ with κ is the wavenumber, $\mathbf{r} = (x, y)^T$ and $\theta \in [0, 2\pi]$. Hence, the real and imaginary parts of the exact solution are defined as

$$\operatorname{Re}(\phi_e(t, x, y)) = A_0 \left(\cos(\mathbf{k} \cdot \mathbf{r} + \varphi) S_1(t) - \sin(\mathbf{k} \cdot \mathbf{r} + \varphi) S_2(t) \right),$$

$$\operatorname{Im}(\phi_e(t, x, y)) = A_0 \left(\cos(\mathbf{k} \cdot \mathbf{r} + \varphi) S_2(t) + \sin(\mathbf{k} \cdot \mathbf{r} + \varphi) S_1(t) \right).$$

In all our simulations for this example, we use $v = 3000$, $\rho = 1$, $\beta = 5$, $f_{s,\ell} = 20$, $T = 1$, $t_s^{(\ell)} = T/2$, $\theta = \pi/4$, $\varphi = \pi/3$, $\kappa = 6\pi$ and $A_0 = 1$. The main aim of this test example is to determine the numerical convergence rates associated with the real part of the exact and approximate solutions at time $t = 1$ using our method for varying degrees of the \mathbb{B}_γ -spline functions. The second objective of this example is to evaluate the accuracy of the proposed method in terms of the L^2 -error with respect to the values of the wavenumber κ . In this example we also explore the benefits of using \mathbb{B}_γ -spline functions with higher degrees as the wavenumber κ increases.

In Table 2 we present the L^2 -error and the corresponding convergence rates obtained using meshes with different densities and different \mathbb{B}_γ -spline orders. It is clear that refining the mesh results in a decrease in the L^2 -error for all considered values of the \mathbb{B}_γ -spline orders. These results also confirm the theoretical convergence of the proposed method for this test example. Indeed, the numerical results in Table 2 demonstrate

Table 3: L^2 -errors for the example of time-Reicker wavelet problem using different wavenumbers and different \mathbb{B}_γ -spline orders.

γ	$\kappa = 2\pi$	$\kappa = 4\pi$	$\kappa = 8\pi$	$\kappa = 16\pi$	$\kappa = 32\pi$	$\kappa = 64\pi$
1	2.9564937E-04	1.1724170E-03	4.6757846E-03	1.8665095E-02	7.4393914E-02	2.9555217E-01
2	9.6817625E-07	7.8094823E-06	6.3811428E-05	5.4269613E-04	5.2435545E-03	7.3517379E-02
3	8.6953517E-09	1.3973869E-07	2.2747967E-06	3.8907725E-05	7.8989910E-04	2.6474106E-02
4	7.5714996E-11	2.4395289E-09	8.0124333E-08	2.8206487E-06	1.2314172E-04	9.5093460E-03
5	7.4535331E-13	4.3833320E-11	2.9040089E-09	2.1148820E-07	2.0348078E-05	3.7783809E-03
6		4.3744986E-12	1.0292256E-10	1.5617220E-08	3.2850967E-06	1.4767031E-03
7			7.2024826E-11	1.1746477E-09	5.4309610E-07	5.7011500E-04
8					8.8949212E-08	2.3078440E-04
9						8.8594761E-05
10						4.2882233E-05

that the calculated convergence orders for the considered values of $\gamma = 1, 2, \dots, 9$ remain consistent with the theoretical order $\mathcal{O}(h^{\gamma+1})$ established in Theorem 5. Next, we examine the accuracy of the proposed spline finite element method for this problem using different values of the wavenumber κ . To this end we set the computational domain $\Omega = [0, 1] \times [0, 1]$ discretized into a fixed mesh with $n_1 = n_2 = 80$ and we vary the values of the wavenumber κ and \mathbb{B}_γ -spline order γ . The obtained results for the L^2 -error are summarized in Table 3 for the selected values of κ and γ . It is clear that the L^2 -error decreases as the \mathbb{B}_γ -spline order γ increases for all selected values of the wavenumber κ . However, a rapid decrease is detected for low wavenumbers and the L^2 -error exhibits larger values for high wavenumbers. For instance, a \mathbb{B}_γ -spline order of $\gamma = 5$ is sufficient to obtain the lowest error for $\kappa = 2\pi$ however, this order needs to reach $\gamma = 10$ for the L^2 -error to attend the lowest value at the high wavenumber $\kappa = 64\pi$. Note that once the lowest value of the L^2 -error is reached for each value of the wavenumber κ no further improvement has been observed when increasing the \mathbb{B}_γ -spline order γ and the error remains stagnated around this lowest value. This behavior is expected as for the L^2 -error to decrease further at those orders, one needs to refine the mesh as well. Overall, the results consistently demonstrate a convergence order of $\mathcal{O}(h^{\gamma+1})$ for the proposed spline finite element method solving this problem.

5.3. Time-progressive wave problem

Our next example solves the problem of recovering a time-progressive plane wave in a squared domain. Here, we solve the wave equations (1)-(3) in the domain $\Omega = [0, 2] \times [0, 2]$ with constant wave speed $v = 3000$, $\rho = 2$, $\beta = 3$ and subject to the initial conditions

$$\phi_0(x, y) = A_0 e^{i(\kappa r^2 + \varphi)}, \quad \text{and} \quad \phi_1(x, y) = 0,$$

where $r = \sqrt{(x-1)^2 + (y-1)^2}$. The source term f , the boundary function g are calculated such that the analytical solution of the problem (1)-(3) is given by

$$\phi_e(x, y, t) = A_0 e^{i(\kappa r^2 + \varphi) - \delta t^2}.$$

Hence, the real and imaginary parts of the exact solution are defined as

$$\text{Re}(\phi_e(t, x, y)) = A_0 \cos(\kappa r^2 + \varphi) e^{-\delta t^2},$$

$$\text{Im}(\phi_e(t, x, y)) = A_0 \sin(\kappa r^2 + \varphi) e^{-\delta t^2}.$$

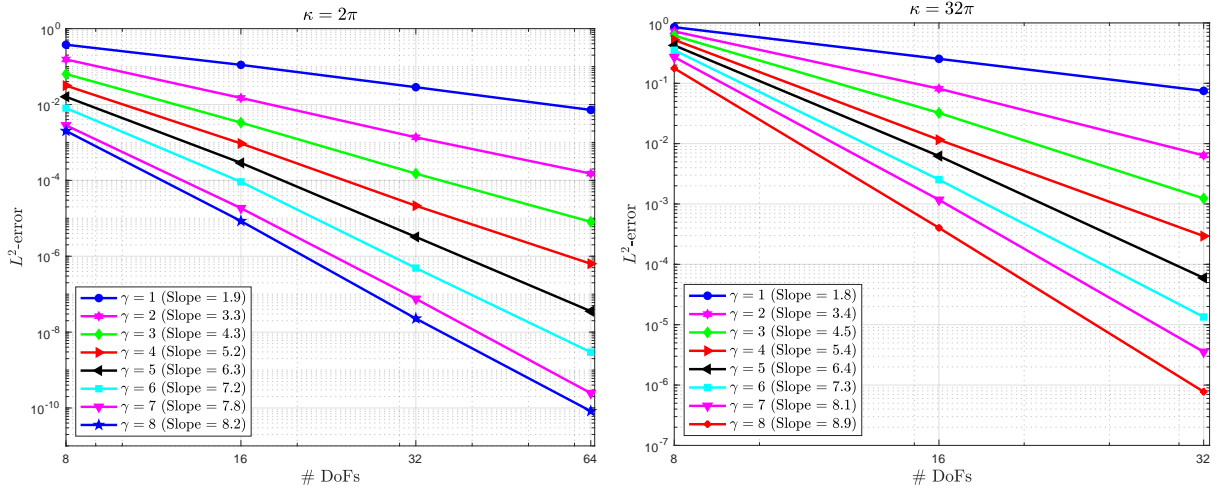


Figure 2: Convergence results for the example of time-progressive wave problem using $\kappa = 2\pi$ (left plot) and $\kappa = 32\pi$ (right plot).

As in the previous examples, we assess the accuracy of the frequency-domain method in this problem by calculating the L^2 -error in the real and imaginary parts of the obtained solutions at the final time $t = 1$ using different mesh densities and \mathbb{B}_γ -spline orders. In all our simulations for this example, $A_0 = 1$, $\varphi = \pi/3$ and $\delta = \pi$. We also examine the accuracy of the proposed method in terms of the L^2 -error with respect to values of the wavenumber κ varying from $\kappa = 2\pi$ to $\kappa = 80\pi$. Note that at high values of the wavenumber κ , the wave is expected to illustrate complex wave features and the problem becomes computationally very challenging and most conventional finite element methods would fail to resolve these wave patterns. This test example aims to evaluate the potential advantages of adopting higher degrees of the \mathbb{B}_γ -spline for solving wave problems at high wavenumbers.

In Figure 2 we illustrate the obtained results for the L^2 -error using different meshes and different \mathbb{B}_γ -spline orders at two different wavenumbers namely, $\kappa = 2\pi$ and $\kappa = 32\pi$. In this figure, we also include the convergence rates referred to by slopes of each error plot. It is clear that setting the \mathbb{B}_γ -spline order γ at a given value and refining the mesh step h yields a substantial decrease in the computed L^2 -error for this example. Comparing the convergence rates in Figure 2, it can be clearly seen that the expected theoretical order of convergence is attended for each \mathbb{B}_γ -spline order γ used in our simulations. It should also be stressed that these convergence rates have not been affected by the increase in the values of the wavenumber, and the same convergence order of the proposed method is preserved almost for the selected wavenumbers $\kappa = 2\pi$ and $\kappa = 32\pi$. It should be mentioned that other numerical simulations, which are not presented here for brevity, were also performed using other wavenumbers outside this range, and the obtained results show the same convergence features.

Next, to evaluate the performance of the proposed method for solving this test problem at high wavenumbers, we summarize in Table 4 the results for the L^2 -error obtained on a fixed mesh with $n_1 = n_2 = 40$ and varying the values of the wavenumber κ and \mathbb{B}_γ -spline order γ . As in the previous example, the L^2 -error clearly decreases as the \mathbb{B}_γ -spline order γ increases for all selected values of the wavenumber κ with a rapid decrease for low wavenumbers compared to high wavenumbers. For the considered wave conditions, it is clear that a \mathbb{B}_γ -spline order of $\gamma = 7$ is sufficient to obtain the lowest L^2 -error for $\kappa = 2.5\pi$ whereas, this order needs to reach $\gamma = 10$ for the L^2 -error to attend the lowest value at the high wavenumber $\kappa = 80\pi$. Again, no further improvement is expected in the L^2 -error once the lowest value of this error is attended for the considered wavenumber and the L^2 -error remains stagnated around this lowest value. In these cases, finer meshes are required in the simulations to allow further improvements in the L^2 -error for increased \mathbb{B}_γ -spline order γ . It is evident from the obtained results that for the considered values of the wavenumber κ ,

Table 4: L^2 -errors for the example of time-progressive wave problem using different wavenumbers and different \mathbb{B}_γ -spline orders.

γ	$\kappa = 2.5\pi$	$\kappa = 5\pi$	$\kappa = 10\pi$	$\kappa = 20\pi$	$\kappa = 40\pi$	$\kappa = 80\pi$
1	2.3331396E-04	8.2748826E-04	2.9703155E-03	1.1240098E-02	4.4314381E-02	1.7557416E-01
2	2.7934498E-07	2.4621633E-06	3.0901882E-05	4.5468310E-04	7.6397201E-03	1.6035738E-01
3	6.2017082E-08	5.9768221E-07	7.5370048E-06	1.1590639E-04	2.1384581E-03	5.3024348E-02
4	2.3709940E-10	3.2672205E-09	1.0417749E-07	4.9320487E-06	3.3093832E-04	4.0979917E-02
5	2.2955488E-10	5.1512329E-10	1.7363996E-08	9.5679000E-07	8.5936601E-05	1.7076387E-02
6	5.5444037E-10	1.0213423E-09	2.1284767E-09	6.3392394E-08	1.6846715E-05	1.1096723E-02
7	1.0211682E-09	1.9705522E-09	3.9485556E-09	1.0545714E-08	4.4451688E-06	5.5065807E-03
8		4.0667873E-09	6.9168717E-09	1.3323539E-08	8.4416772E-07	3.1576824E-03
9					2.2009373E-07	1.5374259E-03
10						7.6682316E-04

the expected convergence rates of $\mathcal{O}(h^{\gamma+1})$ are also preserved for the proposed spline finite element method solving this wave problem.

5.4. A time-Hankel wave problem

For this wave problem we first define the Bessel functions of the first kind J_0 and the second kind Y_0 in their integral forms by

$$J_0(\zeta) = \frac{1}{2} \int_{-1}^1 \cos\left(\zeta \sin\left(\frac{\pi}{2}\theta\right)\right) d\theta, \quad \text{and} \quad Y_0(\zeta) = -\frac{1}{\pi} \int_{-\infty}^{+\infty} \cos(\zeta \cosh(t)) dt, \quad \text{for } \zeta > 0.$$

Then, we reconstruct the zeroth-order Hankel function of first kind $H_0^{(1)}$ as

$$H_0^{(1)}(\zeta) = J_0(\zeta) + iY_0(\zeta).$$

The problem statement for this wave problem consists of solving the equations (1)-(3) in the spatial domain $\Omega = [0, 1] \times [0, 1]$ with a constant wave speed $v = 3000$, $\rho = 2$, $\beta = 3$ and subject to the following initial conditions

$$\phi_0(x, y) = H_0^{(1)}(\kappa r), \quad \text{and} \quad \phi_1(x, y) = H_0^{(1)}(\kappa r)(-i\delta),$$

where κ is the wavenumber and $r = \sqrt{(x - x_s)^2 + (y - y_s)^2}$ is the radial distance to the source position. The source term f and the boundary function g are calculated such that the analytical solution of this test problem is a progressive plane wave given by

$$\phi_e(x, y, t) = H_0^{(1)}(\kappa r)e^{-i\delta t},$$

and its real and imaginary parts are defined as

$$\text{Re}(\phi_e(x, y, t)) = J_0(\kappa r) \cos(\delta t) + Y_0(\kappa r) \sin(\delta t),$$

$$\text{Im}(\phi_e(x, y, t)) = Y_0(\kappa r) \cos(\delta t) - J_0(\kappa r) \sin(\delta t).$$

In all our computations for this example, $A_0 = 1$, $\delta = \frac{\pi}{3}$, $x_s = 1.25$, $y_s = 0.5$ and the obtained results are presented at the final time $t = 1.5$. In Figure 3 we illustrate snapshots of the real and imaginary parts of

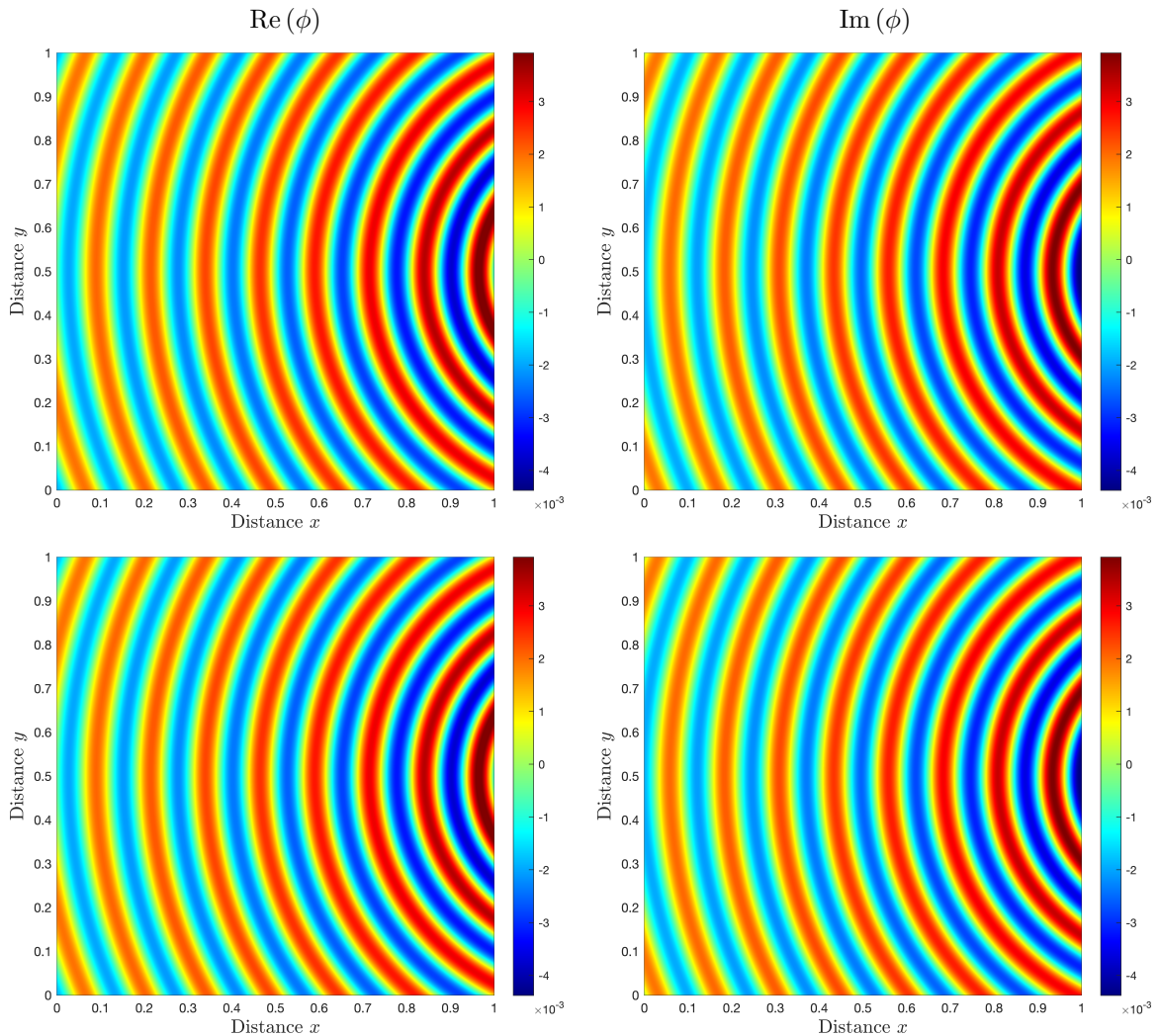


Figure 3: Results for the real and imaginary parts of the analytical solution (first row) and the numerical solution (second row) obtained for the time-Hankel wave problem at time $t = 1.5$ using $\gamma = 9$ and $\kappa = 8\pi$.

the analytical and numerical solutions obtained on a mesh with $n_1 = n_2 = 16$ at time $t = 1.5$ using $\gamma = 9$ and $\kappa = 8\pi$. As expected for this time-dependent wave problem, the Hankel source generates plane waves propagating in the computational domain exhibiting complex patterns once released. These wave patterns are very well captured by the proposed spline finite element method as the small wave features are also well resolved using our method. For the considered wave conditions, it has been observed that the L^2 -error is of orders $\mathcal{O}(1.785109 \times 10^{-8})$ and $\mathcal{O}(5.407296 \times 10^{-8})$ in the real and imaginary parts of the solution, respectively. It should be noted that despite using a relatively coarse mesh in our simulations, the proposed spline finite element method accurately captures these wavefronts and their changes in time. Notice that results obtained using other \mathbb{B}_γ -spline orders reveal the same wave structures and therefore are not included in Figure 3. Again the high accuracy of the proposed approach can be clearly seen from the presented results.

For comparison reasons, we also display in Figure 4 the horizontal cross-sections at $x = 0.5$ of real parts of the analytical and numerical solutions obtained for the time-Hankel wave problem at time $t = 1.5$ using $\kappa = 8\pi$ and different \mathbb{B}_γ -spline orders with two meshes with $n_1 = n_2 = 16$ and $n_1 = n_2 = 20$. It is clear

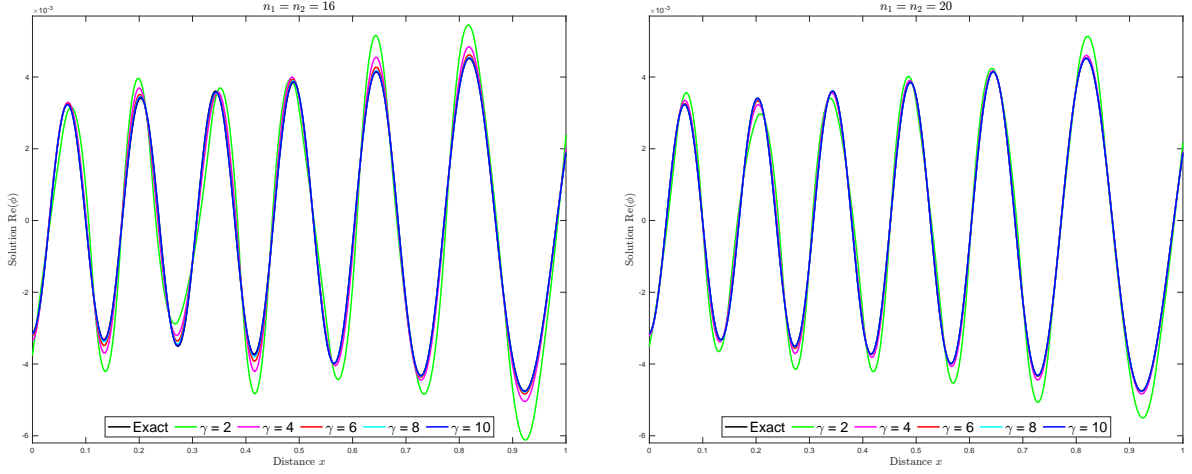


Figure 4: Horizontal cross-sections at $x = 0.5$ of real parts of the analytical and numerical solutions obtained for the time-Hankel wave problem with $n_1 = n_2 = 16$ (left plot) and $n_1 = n_2 = 20$ (right plot) at time $t = 1.5$ using $\kappa = 8\pi$ and five different \mathbb{B}_γ -spline orders.

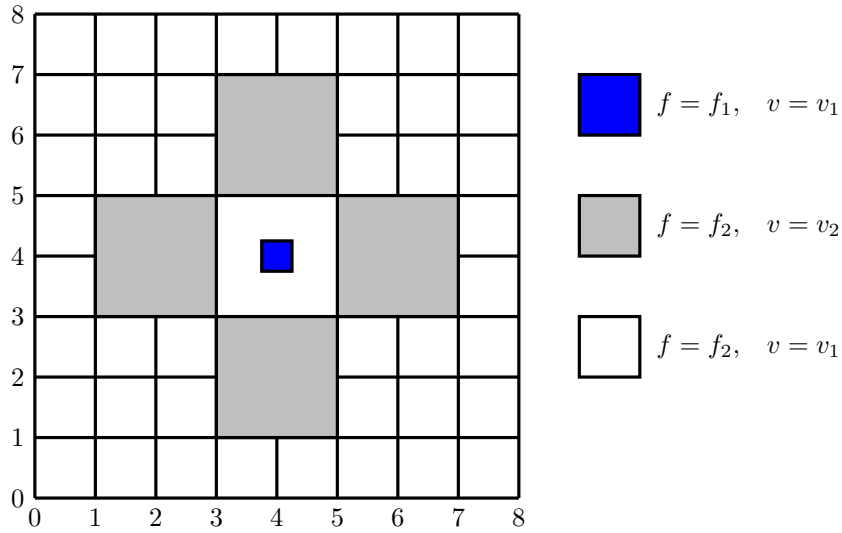


Figure 5: Configuration of the computational domain for the problem of transmission of waves through non-homogeneous materials. Here, values of the wave speed v and source term f are also given according to the specific color used in each area.

that increasing the \mathbb{B}_γ -spline order γ results in an increase of accuracy in both real and imaginary parts of the computed solutions. The results also reveal a consistent behaviour of the error which, up to a certain value of the \mathbb{B}_γ -spline order, remains similar to the errors obtained using the highest value $\gamma = 10$ with some advantage in the computational efficiency for the low values of the \mathbb{B}_γ -spline order. It should be stressed that the accuracy in standard finite element methods for this case is mainly dependent on the element size where only refining the mesh improves the errors. Furthermore, as the wave width becomes smaller at $\kappa = 8\pi$ the error in these methods becomes larger. This is expected as finer meshes are needed in the simulations to capture the narrower wave pulses using the conventional finite element methods. For our approach, using the same coarse mesh and only changing the \mathbb{B}_γ -spline order for different wavenumbers is a particularly useful feature of the proposed spline finite element method, compare the good convergence shown in Figure 4. Otherwise using the standard finite element methods, increasing values of the wavenumber κ would require

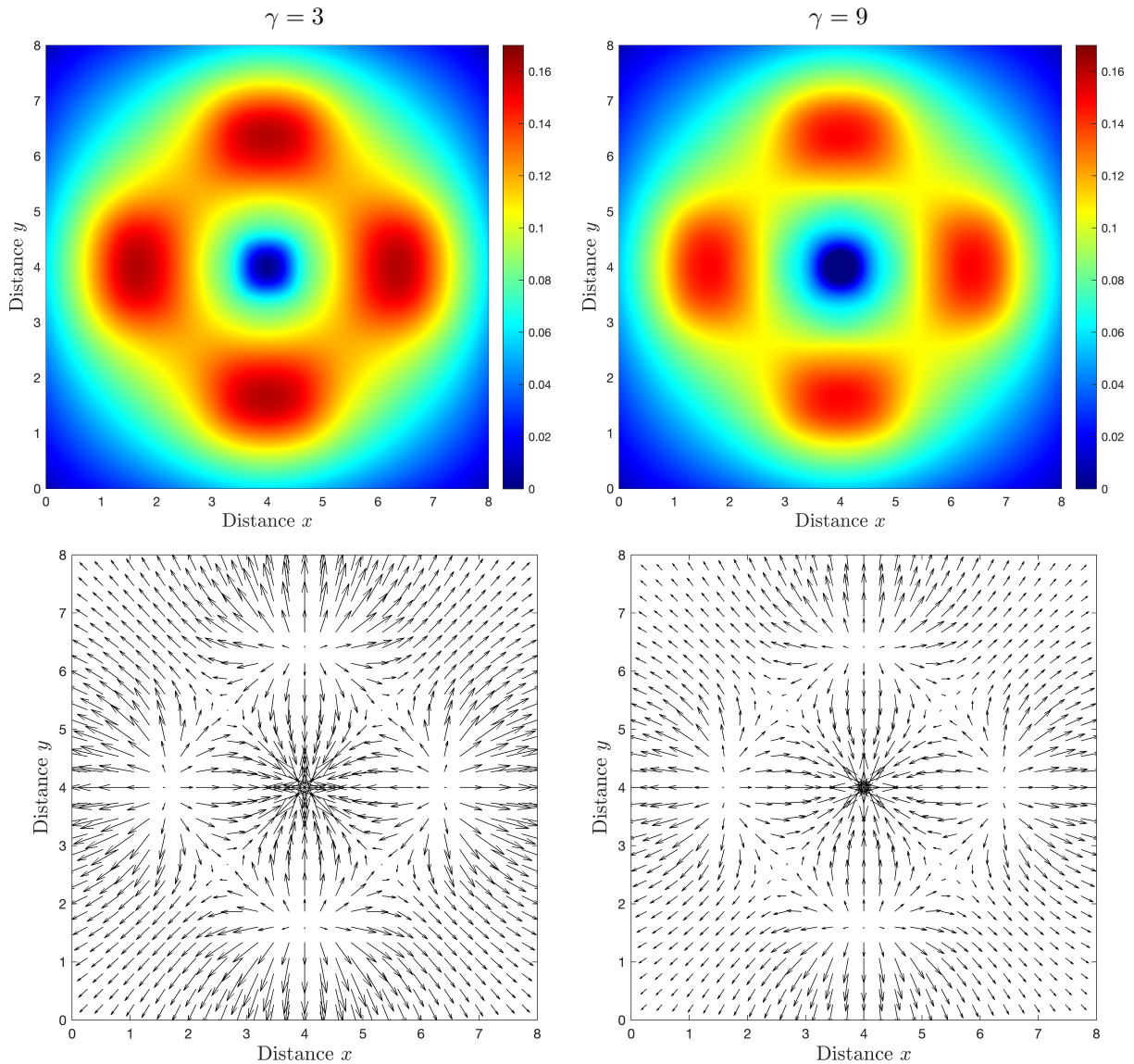


Figure 6: Results for the density magnitude (first row) and the electrical field (second row) obtained for the problem of transmission of waves through non-homogeneous materials at time $t = 1$ using $\gamma = 3$ (first column) and $\gamma = 9$ (second column).

refining the mesh which results in a substantial increase in the computational cost.

5.5. Transmission of waves through non-homogeneous materials

In this final example we examine the performance of the proposed high-order spline finite element method to solve wave problems in non-homogeneous materials. In such problems, numerical modeling plays a crucial role in understanding and analyzing natural phenomena or industrial processes that encompass various scales of interest. This class of applications holds both fundamental and practical significance. Challenges involving heterogeneous media, such as transport processes in porous or disordered media [58], biomedicine [59], and remote sensing [60], frequently exhibit these diverse scales. For instance, the analytical expression of a seismic moment source is generally given by a function that describes the variation of seismic moment depending on both time and space. This function can be adapted depending on the specific characteristics

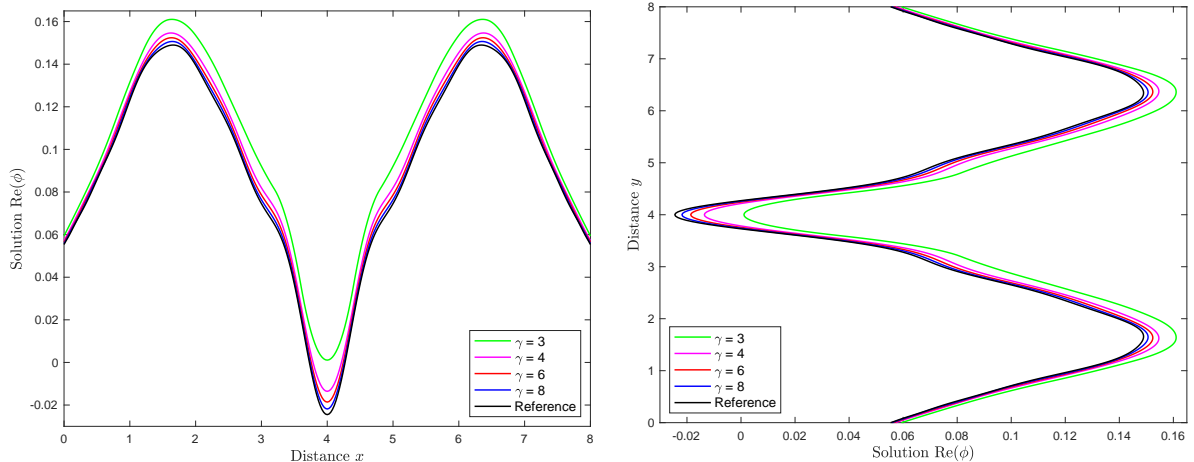


Figure 7: Horizontal cross-sections at $x = 4$ (left plot) and vertical cross-sections at $y = 4$ (right plot) of real parts of the analytical and numerical solutions obtained for the problem of transmission of waves through non-homogeneous materials at time $t = 1$ using four different \mathbb{B}_γ -spline orders.

of the seismic source. In this case, the total seismic moment $M_0(x, y)$ released during the earthquake is defined as the product of the seismic moment magnitude M_ω and a geophysical constant μ that depends on the material properties and the fault geometry. Thus, the analytical expression of the time-dependent seismic moment source $f(x, y, t)$ is often written as

$$f(x, y, t) = M_0(x, y) \mathcal{N}_{(t_s, \sigma^2)}(t),$$

where $\mathcal{N}_{(t_s, \sigma^2)}(t)$ is the source function that describes variation of the seismic moment as a time-dependent function. In general, the source function $\mathcal{N}_{(t_s, \sigma^2)}(t)$ depends on the chosen model to represent release of the seismic energy over time. In addition, one of the most commonly used source function is the Gaussian pulse which is a probability density of the normal law for random variables and it can be defined by

$$\mathcal{N}_{(t_s, \sigma^2)}(t) = \frac{1}{\sqrt{2\pi}\sigma} e^{-\frac{(t-t_s)^2}{2\sigma^2}},$$

where σ is the dispersion coefficient which determines the width of the pulse and t_s is the time center. Note that the above expression represents an idealized seismic source in the form of a Gaussian pulse. In practice, seismic sources can be much more complex and often require more detailed models to account for fault geometry, rupture, and wave propagation. In our simulations for this example, we solve the wave equations (1)-(3) in the spatial domain $\Omega = [0, 8] \times [0, 8]$ subject to homogeneous initial and boundary conditions with $\rho = 2$ and $\beta = 3$. The medium is assumed to be non-homogeneous divided into discontinuous areas as depicted in Figure 5 with the source function

$$f(x, y, t) = \begin{cases} f_1 = \frac{1}{2\pi\nu_1\nu_2} e^{-\left(\frac{(x-x_s)^2}{\nu_1^2} + \frac{(y-y_s)^2}{\nu_2^2}\right)} \mathcal{N}_{(t_s, \sigma^2)}(t), & \text{if } (x, y) \in \Omega_0, \quad t \leq T, \\ f_2 = 0, & \text{if } (x, y) \in \Omega \setminus \Omega_0, \quad t > T, \end{cases}$$

where $\Omega_0 = [3.75, 4.25] \times [3.75, 4.25]$, $x_s = y_s = 4$, $\nu_1 = 1/6$, $\nu_2 = 1/6$, $\sigma = 0.2$, $t_s = T/2$ and $T = 2$. In this example we also assume variable wave speed depending on the spatial location and defined as shown in Figure 5 with $v_1 = 3000$ and $v_2 = 5$.

Figure 6 depicts results for the density magnitude $\phi(x, y, t)$ and the electrical field $\nabla\phi(x, y, t)$ obtained at time $t = 1$ using the \mathbb{B}_γ -spline orders $\gamma = 3$ and $\gamma = 9$ on a mesh with $n_1 = n_2 = 20$. As can be seen

Table 5: L^2 -errors for the problem of transmission of waves through non-homogeneous materials using different \mathbb{B}_γ -spline orders.

n	$\gamma = 3$	$\gamma = 4$	$\gamma = 6$	$\gamma = 8$
10	2.71370402E-01	1.06573164E-01	9.87961916E-02	8.60385258E-02
20	3.01976926E-02	2.84318795E-02	2.14476503E-02	1.65761341E-02
40	1.16654976E-02	6.59581582E-03	2.81202966E-03	4.01807898E-04

from these results, wavefronts generated from the source at the speed v_1 hit the heterogeneous materials (colored in gray color in Figure 5) and reflect back at the speed v_2 to merge into a single wave propagating towards the domain boundary. The wavefronts pass each other moving in opposite directions to reach the domain ends and reflected again to meet at the initial pulse location. This pattern is then repeated at the four heterogeneous regions in the computational domain and all reflected waves are focused at the domain center. It is clear that the density magnitude and electrical field are correctly recovered using the proposed high-order spline finite element method with $\gamma = 9$. It is also evident that using $\gamma = 3$, the obtained solutions of both density magnitude and electrical field exhibit excessive numerical diffusion which is hugely reduced by increasing the \mathbb{B}_γ -spline order to $\gamma = 9$ but keeping the computational mesh fixed with $n_1 = n_2 = 20$. A perfect symmetry along the horizontal and vertical centerlines can also be noticed in the obtained results for the considered low and high \mathbb{B}_γ -spline orders. It should also be stressed that this resolution is captured on a relatively coarse mesh and without any mesh refinements implemented at the interfaces between the heterogeneous regions. The proposed spline finite element method performs well for this wave problem in non-homogeneous materials as the generated waves are accurately resolved without requiring highly demanding computational resources.

To compare the numerical results obtained for this example using different \mathbb{B}_γ -spline orders, we present in Figure 7 the horizontal and vertical cross-sections at $x = 4$ and $y = 4$ of real parts of the numerical solutions at time $t = 1$ using four different \mathbb{B}_γ -spline orders namely, $\gamma = 3, 4, 6$ and 8 . For comparison reasons, we also include reference results obtained using a fine mesh with $n_1 = n_2 = 100$ and a \mathbb{B}_γ -spline order of $\gamma = 10$. An increase in the accuracy is clearly obtained when increasing the \mathbb{B}_γ -spline order γ in both cross-sections. This can be clearly seen in the L^2 -errors presented in Table 5 for the considered \mathbb{B}_γ -spline orders. Again, the results and concluding remarks are consistent with those of the previous wave example. As expected, the heterogeneity in the computational domain generates sharp wavefronts in the wave solutions once reaching the four non-homogeneous areas. These wave patterns are very well captured by the proposed high-order spline finite element method and the full symmetry between the horizontal and vertical cross-sections is also well preserved using our method. It should be mentioned that using time integration methods in the conventional finite element methods solving this wave problem would require very fine meshes specially at the internal discontinuous edges in the computational domain. However, once the error in the numerical solution becomes dominated by the temporal errors, refining the mesh would not further reduce the overall errors. Therefore, the convergence in time needs to be checked first in the standard finite element methods by considering smaller time steps and rerunning the analysis. Once the error cannot be further reduced by refining the time step in these methods one may conclude that the solution has converged in time. This analysis is not needed in our high-order approach as no time integration schemes are required in its implementation. Finally, we also note that the proposed spline finite element method is highly attractive for time-dependent electromagnetic waves.

6. Conclusions

In the present study, we have proposed a novel numerical method for solving time-dependent electromagnetic waves and its associated frequency-domain approach. The method consists of employing a class of high-order splines as basis functions in the finite element solution of the wave problem. To deal with the

time in these problems, a Fourier transform and its inverse are used for the time integration which eliminate accumulated errors generated by approximations of time derivatives such as finite difference approximations or Runge-Kutta schemes among others. Partitioned meshes with tensorial spline functions are used for the spatial discretization and a Gauss-Hermite quadrature is implemented for the calculation of the inverse Fourier transform. We have performed a rigorous convergence analysis and established error estimates for the numerical solution in the relevant norms. Algorithmic details of the proposed method along with its implementation for solving time-dependent electromagnetic waves have also been discussed in this study. Several test examples have been presented to examine the performance of these techniques and the obtained computational results supported the conclusion that the proposed method is highly accurate and it can effectively be used to capture the wave motion of the time-dependent electromagnetic waves. Further validations through comparison against experimental measurements and applications to time-dependent electromagnetic waves in complex geometries will also be tackled in the future work. Extension of the proposed method to similar problems in three-dimensional domains using unstructured meshes will also be subject of a future work.

Data availability statement

The data that support the findings of this study are available from the corresponding author upon reasonable request.

Conflict of interest

The authors have no competing interests to declare that are relevant to the content of this paper.

References

- [1] F. Natterer, Reflection imaging without low frequencies, *Inverse Problems* 27 (2011) 1–6.
- [2] W. Liao, On the dispersion, stability and accuracy of a compact higher-order finite difference scheme for 3D acoustic wave equation, *Journal of Computational and Applied Mathematics* 258 (2014) 151–167.
- [3] M. Drolia, M. M. Shadi, O. Laghrouche, M. Seaid, J. Trevelyan, Enriched finite element method for initial-value problem of transverse electromagnetic waves in time domain, *Computer & Structures* 101 (1) (2016) 54–78.
- [4] C. Chu, P. Stoffa, Implicit finite-difference simulations of seismic wave propagation, *Geophysics* 77 (2) (2012) T57–T67.
- [5] W. L. Sambit Das, A. Gupta, An efficient fourth-order low dispersive finite difference scheme for a 2-d acoustic wave equation, *Journal of Computational and Applied Mathematics* 270 (2014) 571–583.
- [6] P. E. Perrey-Debain, J. Trevelyan, P. Bettess, Wave boundary elements: a theoretical overview presenting applications in scattering of short waves, *Engineering Analysis with Boundary Elements* 22 (2004) 131–141.
- [7] A. Buffa, M. Costabel, C. Schwab, Boundary element methods for Maxwell’s equations on non-smooth domains, *Numerische Mathematik* 92 (4) (2002) 679–710.
- [8] A. Buffa, R. Hiptmair, T. v. Petersdorff, C. Schwab, Boundary element methods for Maxwell transmission problems in Lipschitz domains, *Numerische Mathematik* 95 (2003) 459–485.
- [9] J.-F. Lee, R. Lee, A. Cangellaris, Time-domain finite-element methods, *IEEE Transactions on Antennas and Propagation* 45 (3) (1997) 430–442.
- [10] K. S. Yee, Numerical solution of initial boundary value problems involving Maxwell’s equations in isotropic media, *International Journal for Numerical Methods in Engineering* 14 (3) (1966) 302–307.
- [11] K. Mattsson, F. Ham, G. Iaccarino, Stable and accurate wave-propagation in discontinuous media, *Journal of Computational Physics* 227 (2008) 8753–8767.
- [12] H. Sielschott, Measurement of horizontal flow in a large scale furnace using acoustic vector tomography, *Flow Measurement and Instrumentation* 8 (1997) 191–197.
- [13] P. E. Perrey-Debain, J. Trevelyan, P. Bettess, Plane wave interpolation in direct collocation boundary element method for radiation and wave scattering: Numerical aspects and applications, *Journal of Sound and Vibration* 261 (2003) 839–858.
- [14] P. E. Perrey-Debain, J. Trevelyan, P. Bettess, Use of wave boundary elements for acoustic computations, *Journal of Computational Acoustics* 11 (2003) 305–321.
- [15] Y. Ma, J. Yu, Y. Wang, An efficient complex-frequency shifted-perfectly matched layer for second-order acoustic wave equation, *International Journal for Numerical Methods in Engineering* 97 (2014) 130–148.
- [16] J. Thomas, *Numerical partial differential equations: Finite difference methods*, Vol. 22, Springer Science & Business Media, 2013.
- [17] S. Bilbao, B. Hamilton, Higher-order accurate two-step finite difference schemes for the many-dimensional wave equation, *Journal of Computational Physics* 367 (2018) 134–165.

- [18] H. Wang, W. Yang, Y. Huang, Adaptive finite element method for the sound wave problems in two kinds of media, *Computers & Mathematics with Applications* 79 (3) (2020) 789–801.
- [19] M. Gorakifard, I. Cuesta, C. Saluena, E. Far, Acoustic wave propagation and its application to fluid structure interaction using the cumulant lattice boltzmann method, *Computers & Mathematics with Applications* 87 (2021) 91–106.
- [20] C. Jansari, J. Videla, S. Natarajan, S. Bordas, E. Atroshchenko, Adaptive enriched geometry independent field approximation for 2D time-harmonic acoustics, *Computers & Structures* 263 (2022) 106728.
- [21] S. B. G. Karakoc, S. K. Bhowmik, D. Y. Sucu, A novel scheme based on collocation finite element method to generalised Oskolkov equation, *Journal of Science and Arts* 21 (4) (2021) 895–908.
- [22] S. B. Gazi Karakoc, M. Neilan, A C^0 finite element method for the biharmonic problem without extrinsic penalization, *Numerical Methods for Partial Differential Equations* 30 (4) (2014) 1254–1278.
- [23] S. B. G. Karakoc, A numerical analysing of the GEW equation using finite element method, *Journal of Science and Arts* 19 (2) (2019) 339–348.
- [24] W. Zhang, Y. Zhuang, L. Zhang, A new high-order finite volume method for 3D elastic wave simulation on unstructured meshes, *Journal of Computational Physics* 340 (2017) 534–555.
- [25] T. Ghoudi, M. S. Mohamed, M. Seaid, Novel adaptive finite volume method on unstructured meshes for time-domain wave scattering and diffraction, *Computers & Mathematics with Applications* 141 (2023) 54–66.
- [26] A. Deraemaeker, I. Babuška, P. Bouillard, Dispersion and pollution of the FEM solution for the Helmholtz equation in one, two and three dimensions, *International journal for numerical methods in engineering* 46 (4) (1999) 471–499.
- [27] F. Ihlenburg, I. Babuška, Finite element solution of the Helmholtz equation with high wave number Part I: The h-version of the FEM, *Computers & Mathematics with Applications* 30 (9) (1995) 9–37.
- [28] G. C. Diwan, M. S. Mohamed, Pollution studies for high order isogeometric analysis and finite element for acoustic problems, *Computer Methods in Applied Mechanics and Engineering* 350 (2019) 701–718.
- [29] Y. Wang, K. Tamma, D. Maxam, T. Xue, G. Qin, An overview of high-order implicit algorithms for first-/second-order systems and novel explicit algorithm designs for first-order system representations, *Archives of Computational Methods in Engineering* (2021) 1–27.
- [30] M.-J. Lai, L. L. Schumaker, *Spline functions on triangulations*, no. 110, Cambridge University Press, 2007.
- [31] G. Wahba, Spline interpolation and smoothing on the sphere, *SIAM Journal on Scientific and Statistical Computing* 2 (1) (1981) 5–16.
- [32] L. Schumaker, *Spline functions: Basic theory*, Cambridge university press, 2007.
- [33] C. de Boor, *A Practical Guide to Splines*, Springer-Verlag, New York, 1978.
- [34] M. A. Scott, X. Li, T. W. Sederberg, T. J. Hughes, Local refinement of analysis-suitable T-splines, *Computer Methods in Applied Mechanics and Engineering* 213 (2012) 206–222.
- [35] L. L. Schumaker, L. Wang, Approximation power of polynomial splines on T-meshes, *Computer Aided Geometric Design* 29 (8) (2012) 599–612.
- [36] S. B. G. Karakoc, A. Saha, D. Y. Sucu, A collocation algorithm based on septic B-splines and bifurcation of traveling waves for Sawada–Kotera equation, *Mathematics and Computers in Simulation* 203 (2023) 12–27.
- [37] N. M. Yağmurlu, A. S. Karakaş, Numerical solutions of the equal width equation by trigonometric cubic B-spline collocation method based on Rubin–Graves type linearization, *Numerical Methods for Partial Differential Equations* 36 (5) (2020) 1170–1183.
- [38] N. M. Yağmurlu, A. S. Karakaş, A novel perspective for simulations of the MEW equation by trigonometric cubic B-spline collocation method based on Rubin–Graves type linearization., *Computational Methods for Differential Equations* 10 (4) (2022).
- [39] S. Kutluay, N. M. Yağmurlu, A. S. Karakaş, A novel perspective for simulations of the modified equal-width wave equation by cubic Hermite B-spline collocation method, *Wave Motion* 129 (2024) 103342.
- [40] T. Lyche, L. L. Schumaker, Local spline approximation methods, *Journal of Approximation Theory* 15 (4) (1975) 294–325.
- [41] M. Addam, A. B. Abdellah, A. Bouhamidi, Dynamic responses of beam deflection model using γ -splines functions and Fourier transform discretization solvers, *Archives of Computational Methods in Engineering* 30 (4) (2023) 2383–2408.
- [42] M. El-Amrani, A. El Kacimi, B. Khouya, M. Seaid, A Bernstein–Bézier Lagrange–Galerkin method for three-dimensional advection-dominated problems, *Computer Methods in Applied Mechanics and Engineering* 403 (2023) 115758.
- [43] A. El Kacimi, O. Lagrouche, D. Ouazar, M. S. Mohamed, M. Seaid, J. Trevelyan, Enhanced conformal perfectly matched layers for Bernstein–Bézier finite element modelling of short wave scattering, *Computer Methods in Applied Mechanics and Engineering* 355 (2019) 614–638.
- [44] T. J. Hughes, J. A. Cottrell, Y. Bazilevs, Isogeometric analysis: CAD, finite elements, NURBS, exact geometry and mesh refinement, *Computer methods in applied mechanics and engineering* 194 (39-41) (2005) 4135–4195.
- [45] M. Addam, Approximation du problème de diffusion en tomographie optique et problème inverse, Ph.D. thesis, LMPA-ULCO, Université Lille-Nord de France (2010).
- [46] M. Addam, A. Bouhamidi, K. Jbilou, A numerical method for one-dimensional diffusion problem using Fourier transform and the B-spline Galerkin method, *Applied mathematics and computation* 215 (12) (2010) 4067–4079.
- [47] E. Zampieri, L. F. Pavarino, A numerical comparison of Galerkin and collocation isogeometric approximations of acoustic wave problems, *Applied Numerical Mathematics* (2023).
- [48] M. Samuelides, L. Touzillier, *Analyse harmonique*, Éditions Cepaduès, 1990.
- [49] K. Yosida, *Functional analysis*, Vol. 123, Springer Science & Business Media, 2012.
- [50] J. Dieudonné, *Foundations of modern analysis*, Read Books Ltd, 2011.
- [51] V. Brattka, A. Yoshikawa, Towards computability of elliptic boundary value problems in variational formulation, *Journal of Complexity* 22 (2006) 858–880.

- [52] J. L. Lions, E. Magenes, Non-homogeneous Boundary Value Problems and Applications I, Springer, New York, 1972.
- [53] H. Brézis, Analyse Fonctionnelle: Théorie et applications, Dunod, Paris, 1999.
- [54] P. G. Ciarlet, The finite element method for elliptic problems, SIAM, 2002.
- [55] M. H. Schultz, R. S. Varga, *l*-splines, Numerische Mathematik 10 (1967) 345–369.
- [56] M. H. Schultz, Splines Analysis, Prentice-Hall, Englewood cliffs, New Jersey, 1973.
- [57] A. Quarteroni, A. Valli, Numerical approximation of partial differential equations, Vol. 23, Springer Science & Business Media, 2008.
- [58] Y. Edery, A. Guadagnini, H. Scher, B. Berkowitz, Reactive transport in disordered media: Role of fluctuations in interpretation of laboratory experiments, Advances in Water Resources 51 (2013) 86–103.
- [59] P. M. Sloot, A. G. Hoekstra, Multi-scale modelling in computational biomedicine, Briefings in Bioinformatics 11 (1) (2010) 142–152.
- [60] H. Wu, Z.-L. Li, Scale issues in remote sensing: A review on analysis, processing and modeling, Sensors 9 (3) (2009) 1768–1793.



Citation on deposit: El-Barkani, I., El-Hadouti, I., Addam, M., & Seaid, M. (2024). High-order spline finite element method for solving time-dependent electromagnetic waves. *Applied Numerical Mathematics*, 206, 48-74. <https://doi.org/10.1016/j.apnum.2024.08.002>

For final citation and metadata, visit Durham

Research Online URL: <https://durham-repository.worktribe.com/output/2757080>

Copyright statement: This accepted manuscript is licensed under the Creative Commons Attribution 4.0 licence.

<https://creativecommons.org/licenses/by/4.0/>